AtCGL160 recruits chloroplast coupling factor 1

Bennet Reiter[1], Lea Rosenhammer[1], Giada Marino[1], Stefan Geimer[2], Dario Leister[1], Thilo Rühle[1,§]

[1]Plant Molecular Biology Faculty of Biology I, Ludwig-Maximilians-Universität Munich, D-82152 Planegg-Martinsried, Germany (B.R., L.R., G.M., D.L., T.R.)

[2]Zellbiologie/Elektronenmikroskopie NW I/B1, Universität Bayreuth, 95447 Bayreuth, Germany

[§] To whom correspondence should be addressed. E-mail: thilo.ruehle@biologie.uni-muenchen.de

Running title: AtCGL160 links CF_1 to a CF_O assembly module

Abstract

ATP synthases couple the generation of chemical energy to a transmembrane electro-chemical potential. Like ATP synthases in bacteria and mitochondria, chloroplast ATP synthases consist of a membrane-spanning (CF_O) and a soluble coupling factor (CF_1). Accessory factors facilitate subunit production and orchestrate the assembly of the functional CF_1-CF_O complex. It was previously shown that the accessory factor CGL160 promotes the formation of plant CF_O and performs a similar function in the assembly of its c-ring to that of the distantly related bacterial Atp1/UncI protein. In this study, we show that the N-terminal portion of CGL160 (AtCGL160N), which is specific to the green lineage, is required for late steps in CF_1-CF_O assembly in *Arabidopsis thaliana*. In plants that lacked this stroma-exposed domain, photosynthesis was impaired, and amounts of CF_1-CF_O were reduced to about 65% of the wild-type level. Loss of AtCGL160N did not perturb c-ring formation, but led to a 10-fold increase in the numbers of CF_1 sub-complexes in the stroma relative to the wild type and the CF_1 assembly mutant *atcgld11-1*. Co-immunoprecipitation and protein crosslinking assays revealed an association of AtCGL160 with CF_1 subunits. Yeast two-hybrid assays localized the interaction to a stretch of AtCGL160N that binds to the thylakoid-proximal domain of CF_1-β that includes the conserved DELSEED motif. We therefore propose that AtCGL160 has acquired an additional function in the recruitment of soluble CF_1 to a membrane-integral CF_O sub-complex, which is critical for the modulation of CF_1-CF_O activity and photosynthesis in chloroplasts.

Keywords: chloroplast, photosynthesis, ATP synthase, thylakoid complex, assembly, CF_1-CF_O, Arabidopsis

Introduction

F-type ATP synthases, which utilize chemiosmotic membrane potentials to generate ATP, are central actors in the energy metabolism of bacteria, mitochondria and chloroplasts. These biological nanomotors share a largely conserved structure, consisting of a soluble F_1 and a membrane-bound F_O moiety. Bacterial and chloroplast ATP synthases (CF_1-CF_O) are closely related with respect to size and subunit composition (Groth and Pohl, 2001; Vollmar et al., 2009; Hahn et al., 2018) and, in contrast to the multimeric mitochondrial ATP synthases, exist as monomers in thylakoid membranes (Daum et al., 2010). In the chloroplasts of higher plants, CF_1-CF_O complexes reside exclusively in stroma lamellae and grana-end membranes, because the ~16-nm stromal extension of CF_1 prevents its incorporation into the tightly packed grana stacks (Daum et al., 2010).

During photophosphorylation, CF_1-CF_O complexes couple the light-driven generation of the trans-thylakoid proton-motive force (*pmf*) to ADP phosphorylation. The membrane-embedded proteolipidic c_{14}-ring, together with the non-covalently bound central stalk $\gamma\varepsilon$, form the motor unit, and drive rotary catalysis by CF_1. The peripheral stator consists of the subunits a, b and b', and is connected to the $(\alpha\beta)_3$ unit by the δ subunit, which acts as a flexible hinge between CF_1 and CF_O (Murphy et al., 2019). Protons are translocated from the luminal to the stromal side via two aqueous channels in the a subunit. During translocation, each proton enters the access channel and binds to a conserved glutamate residue in subunit c. The c_{14} motor executes an almost complete rotation before releasing the proton into the stroma through the exit channel (Hahn et al., 2018). The counterclockwise rotation of the central stalk in the vicinity of the hexamer triggers alternating nucleotide-binding affinities in the β subunits that ultimately drive ATP generation (reviewed in von Ballmoos et al., 2009; Junge and Nelson, 2015).

As a result of extensive organellar gene transfer during plant evolution, three CF_1-CF_O subunits (b', γ, δ) are encoded in the nuclear genome, while the remaining CF_1-CF_O genes are organized into two plastid operons. Consequently, two different gene-expression systems must be tightly coordinated with the chloroplast protein import machinery for efficient CF_1-CF_O biogenesis. Several CF_1-CF_O auxiliary factors involved in plastid gene expression have been identified, including proteins involved in mRNA processing (AEF1), mRNA stabilization (PPR10, BFA2) and translation initiation (ATP4, TDA1) (Pfalz et al., 2009; Eberhard et al., 2011; Zoschke et al., 2012; Yap et al., 2015; Zhang et al., 2019). Moreover, CF_1-CF_O assembly factors ensure correct complex stoichiometry, and prevent the accumulation of dead-end products or harmful intermediates that could lead to wasteful ATP hydrolysis or *pmf* dissipation.

As in the case of the bacterial assembly model, plastid CF_1-CF_O complexes are constructed from different intermediates or modules (reviewed in Rühle and Leister, 2015). CF_1 assembly was first examined using in-vitro reconstitution assays, and was shown to be initiated by α/β dimerization in a chaperone-assisted process (Chen and Jagendorf, 1994). CF_1 formation depends on CGLD11/BFA3, which is specific to green plants, interacts with the hydrophobic catalytic site of the β-subunit and may prevent aggregation or formation of unfavorable homodimers (Grahl et al., 2016; Zhang et al., 2016). Moreover, PAB (Mao et al., 2015) and BFA1 (Zhang et al., 2018) have been proposed to be required for efficient incorporation of the γ subunit into CF_1.

Less is known about CF_O assembly, and only one accessory factor – CONSERVED ONLY IN THE GREEN LINEAGE 160 (CGL160) – has been identified so far (Rühle et al., 2014). Absence of CGL160 in the *Arabidopsis thaliana* mutant *atcgl160-1* is associated with a significant reduction (70-90%) in wild-type CF_1-CF_O levels, and CF_O-c subunits accumulate as monomers. Moreover, split-ubiquitin assays have provided evidence that AtCGL160 interacts with CF_O-c and CF_O-b. It was therefore concluded that AtCGL160 is required for efficient formation of the c-ring in chloroplasts and shares this function with its distantly related bacterial counterpart Atp1/UncI (Suzuki et al., 2007; Ozaki et al., 2008). Furthermore, AtCGL160 was suggested to participate in CF_1 assembly into the holo-complex, based on CF_1 subcomplex co-migration and crosslinking experiments using a putatively specific anti-AtCGL160 antibody (Fristedt et al., 2015).

In this study, the function of the N-terminal domain that is conserved in all CGL160 proteins from the green lineage was investigated in Arabidopsis. The results demonstrate that this domain (AtCGL160N) mediates the critical connection of CF_1 to CF_O assembly modules by interacting with subunit β. Thus, CGL160 emerges as a key auxiliary factor that not only promotes CF_O formation, but is also involved in late CF_1-CF_O assembly steps.

Results

The N-terminal moiety of AtCGL160 is required for efficient photosynthesis and CF_1-CF_O functionality

CGL160 was identified based on its coregulation with photosynthetic genes in ATTED-II (Obayashi et al., 2009) and its affiliation to the GreenCut suite of proteins (Merchant et al., 2007; Karpowicz et al., 2011). The C-terminal transmembrane segment of CGL160 (~15 kDa) is distantly related to bacterial Atp1/UncI (Rühle et al., 2014; Fristedt et al., 2015), whereas the larger N-terminal portion of the protein sequence is only conserved in algae, bryophytes, and

108 higher plants (Supplemental Fig. 1). This latter domain of ~200 amino acids (aa) in *Arabidopsis*
109 *thaliana* (AtCGL160N) includes a predicted N-terminal chloroplast transit peptide (cTP) of 46
110 aa (Emanuelsson et al., 1999), and mass spectrometry has identified several phosphorylated
111 peptides which are derived from positions 106-134 (Reiland et al., 2009; Reiland et al., 2011;
112 Roitinger et al., 2015). Indeed, two conserved putative phosphorylation sites were found in a
113 multiple sequence alignment of CGL160 homologs from species across the green lineage,
114 which correspond to positions S111 and S126 in AtCGL160 (Fig. 1, Supplemental Fig. 1).

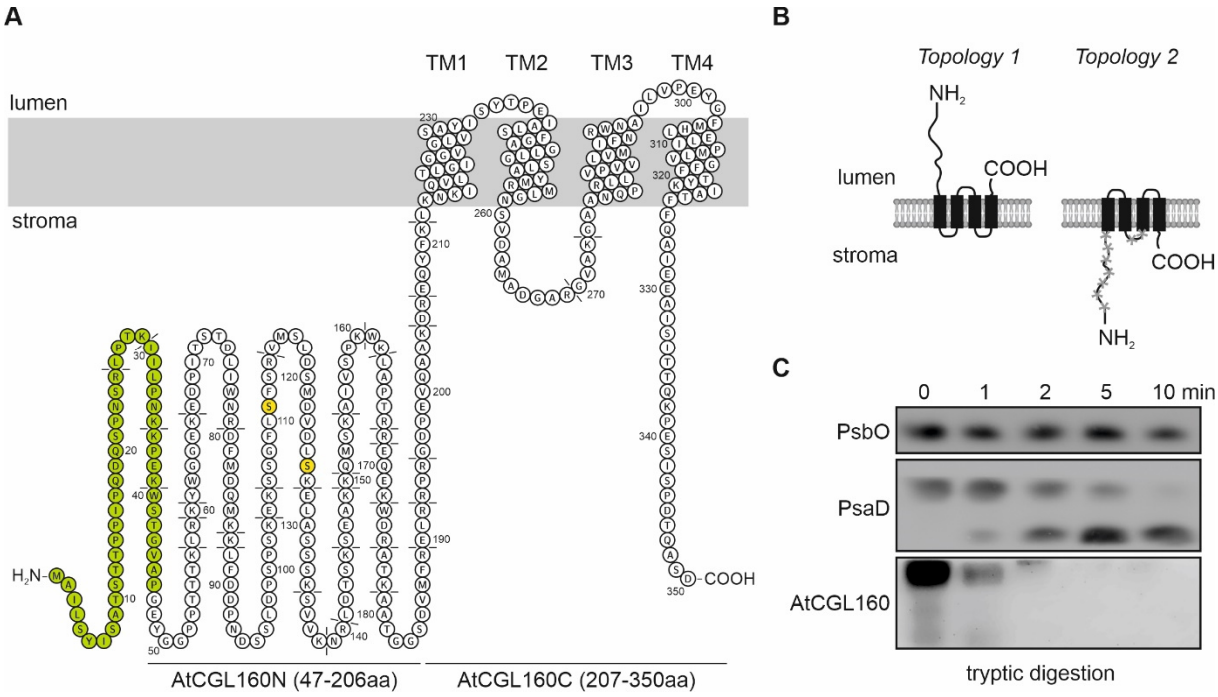

115

116 **Figure 1. Topology of AtCGL160 and trypsin cleavage-site prediction. A,** Transmembrane
117 (TM) domain predictions were obtained from the AtCGL160 UniProt protein accession
118 O82279. Putative trypsin cleavage sites are highlighted in dashed lines and amino-acid
119 positions are indicated. The topology was drawn for the full-length sequence of AtCGL160
120 including the predicted transit peptide (green) with Protter (Omasits et al., 2014). Two
121 conserved serine residues (S111 and S126) are marked in yellow. **B,** Representation of two
122 putative AtCGL160 topologies. The four transmembrane domains are indicated as black
123 boxes. Accessible trypsin digestion sites are highlighted by grey stars. **C,** Immunoblot of
124 thylakoid membranes of the WT (Col-0) fractionated by SDS-PAGE, untreated (0 min) or
125 treated with trypsin for 1, 2, 5 and 10 min. Blots were probed with antibodies against the lumen-
126 oriented PSII subunit PsbO, the stroma-exposed PSI subunit PsaD and AtCGL160.
127

128 Earlier studies have provided experimental evidence for the localization of AtCGL160 to the
129 thylakoid membrane (Rühle et al., 2014; Tomizioli et al., 2014; Fristedt et al., 2015). To gain
130 further insights into the topology of AtCGL160, a protease protection assay was carried out
131 (Fig. 1B, C). In the case of topology 1, all trypsin cleavage sites in AtCGL160 reside in the
132 lumen of the thylakoid and remain fully protected from proteolytic degradation (Fig. 1B).
133 Conversely, the stromal orientation of AtCGL160N predicted for topology 2 would expose
134 trypsin cleavage sites and lead to degradation products of less than 2 kD (Fig. 1A). To test the
135 accessibility of native AtCGL160N, wild-type thylakoids were isolated and treated with trypsin

for 10 min (Fig. 6B). As expected, the luminal PSII subunit PsbO was not affected by the enzyme, whereas the stromally exposed PSI subunit PsaD was susceptible to the protease. AtCGL160N was also efficiently digested, leaving no detectable proteolytic cleavage products, which is consistent with protrusion of the entire N-terminal domain into the stroma, as shown in topology 2 (Fig. 6A).

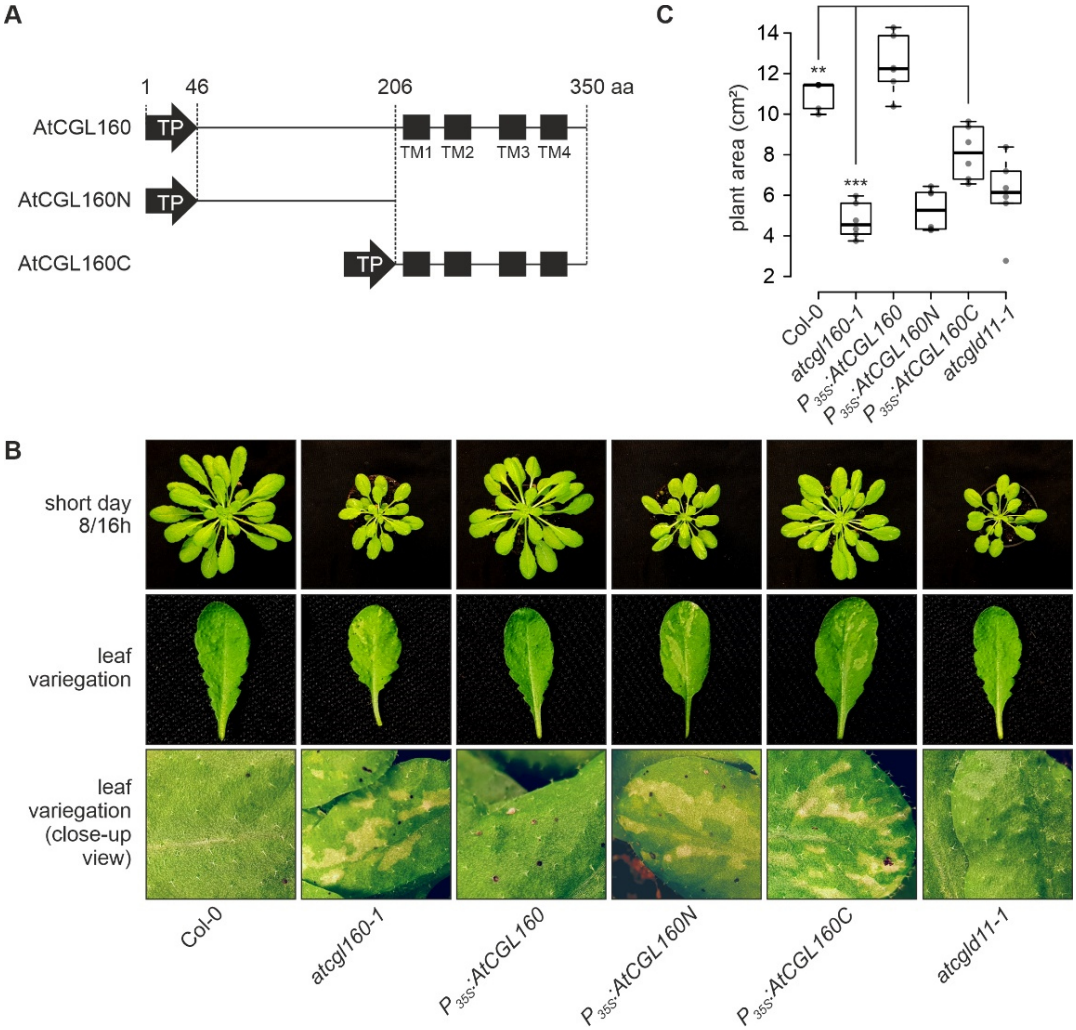

Figure 2. Growth phenotype and leaf variegation of *P_{35S}:AtCGL160, P_{35S}:AtCGL160N* and *P_{35S}:AtCGL160C* plants under short-day conditions. A, Schematic representations of reintroduced AtCGL160 coding sequences. Plants lacking AtCGL160 were transformed with overexpressor constructs harboring the coding sequences for the full-length AtCGL160 (*P_{35S}:AtCGL160*) and its N- (*P_{35S}:AtCGL160N*) and C-terminal (*P_{35S}:AtCGL160C*) segments. Transcription was under the control of the 35S CaMV promoter and targeting to the chloroplast was mediated by the transit peptide of AtCGL160 (TP). Amino-acid positions are indicated and predicted transmembrane domains (TM1-TM4) are schematically shown as black boxes. **B**, Leaf morphology of Col-0, *atcgl160-1*, *P_{35S}:AtCGL160, P_{35S}:AtCGL160N*, *P_{35S}:AtCGL160C* and *atcgld11-1* plants. **C**, Leaf areas of 6 individual plants per genotype were determined 4 weeks after germination. The horizontal lines represent the median, and boxes indicate the 25th and 75th percentiles. Whiskers extend the interquartile range by a factor of 1.5×, and outliers are represented by dots. The effect of the deletion of AtCGL160N in *P_{35S}:AtCGL160C* plants on growth under short-day conditions was tested by paired sample t-test (two-sided). Statistically significant differences are marked with asterisks (**P*<0.05, ***P*<0.01, and ****P*<0.001).

158 To dissect the function of the N-terminal portion of AtCGL160, three different constructs under
159 control of the 35S promoter were cloned, transformed into the *atcgl160-1* background and
160 screened for complementation (Fig. 2, Supplemental Fig. 2A). Plants that overexpressed the
161 full-length coding sequence (CDS) of *AtCGL160* served as controls (P_{35S}*:AtCGL160*), while
162 the other two genotypes expressed either the CDS of the N-terminal (P_{35S}*:AtCGL160N*) or the
163 C-terminal segment (P_{35S}*:AtCGL160C*) of the protein (Supplemental Fig. 2B, C). In the case of
164 P_{35S}*:AtCGL160C* plants, targeting of the truncated version to chloroplasts was achieved by
165 fusing the CDS of the AtCGL160-derived cTP (1-46 aa) to that of AtCGL160C (Fig. 2A). As
166 was previously demonstrated in complementation analyses with P_{35S}*:AtCGL160-eGFP* lines
167 (Rühle et al., 2014), overexpression of the full-length *AtCGL160* rescued the *atcgl160-1*
168 phenotype (Supplemental Fig. 2A), as indicated by wild-type-like growth and restored leaf
169 morphology under short-day conditions (Fig. 2B, C). P_{35S}*:AtCGL160N* failed to complement
170 the mutant phenotype (Fig. 2B, C, Supplemental Fig. 2A) and AtCGL160N could not be
171 detected in either stromal or thylakoid extracts (Supplemental Fig. 3). Since *AtCGL160N*
172 transcripts were present in WT-like amounts in P_{35S}*:AtCGL160N* plants (Supplemental Fig.
173 2C), the lack of AtCGL160N is probably due to proteolytic degradation owing to its inability to
174 associate correctly with thylakoids. Nevertheless, P_{35S}*:AtCGL160N* plants were retained and
175 served as an additional AtCGL160 knockout control. P_{35S}*:AtCGL160C* plants with similar
176 overexpression rates to P_{35S}*:AtCGL160* plants (Supplemental Fig. 2B, C) were characterized
177 by a significant increase in leaf area compared to the mutant background *atcgl160-1*, but were
178 growth-retarded with respect to the wild-type control. Interestingly, like *atcgl160-1*,
179 P_{35S}*:AtCGL160C* plants developed a variegated phenotype in old leaves, which was not found
180 either in the wild type or in the CF_1 assembly mutant *atcgld11-1* (Grahl et al., 2016) under
181 short-day conditions (Fig. 2B).
182 To analyze the leaf phenotype in more detail, we carried out electron microscopic analyses of
183 Col-0, *atcgl160-1* and P_{35S}*:AtCGL160C* plants (Fig. 3). In these genotypes, the chloroplast
184 ultrastructure in preparations from green leaf sections was unchanged with regard to thylakoid
185 content, curvature and grana organization (Fig. 3 A-F). These observations in *atcgl160-1*,
186 together with previous ultrastructural analyses of the CF_1 assembly mutant line *atcgld11-1*
187 (Grahl et al., 2016) and spinach chloroplasts (Daum et al., 2010), support the idea that CF_1-
188 CF_O complexes are not physically involved in thylakoid curvature formation. Examination of
189 white leaf sections in *atcgl160-1* and P_{35S}*:AtCGL160C* revealed the absence of thylakoids in
190 plastids, accompanied by the appearance of plastoglobuli in densely packed stromal clusters
191 (Fig. 3 G-J). Furthermore, large vesicles were observed, which also point to increased
192 catabolic activity and degradation processes in *atcgl160-1* and P_{35S}*:AtCGL160C* plastids.
193 Another finding was the inclusion of mitochondria in degraded plastids, which was also
194 observed, to a lesser extent, in white leaf sectors of P_{35S}*:AtCGL160C*.

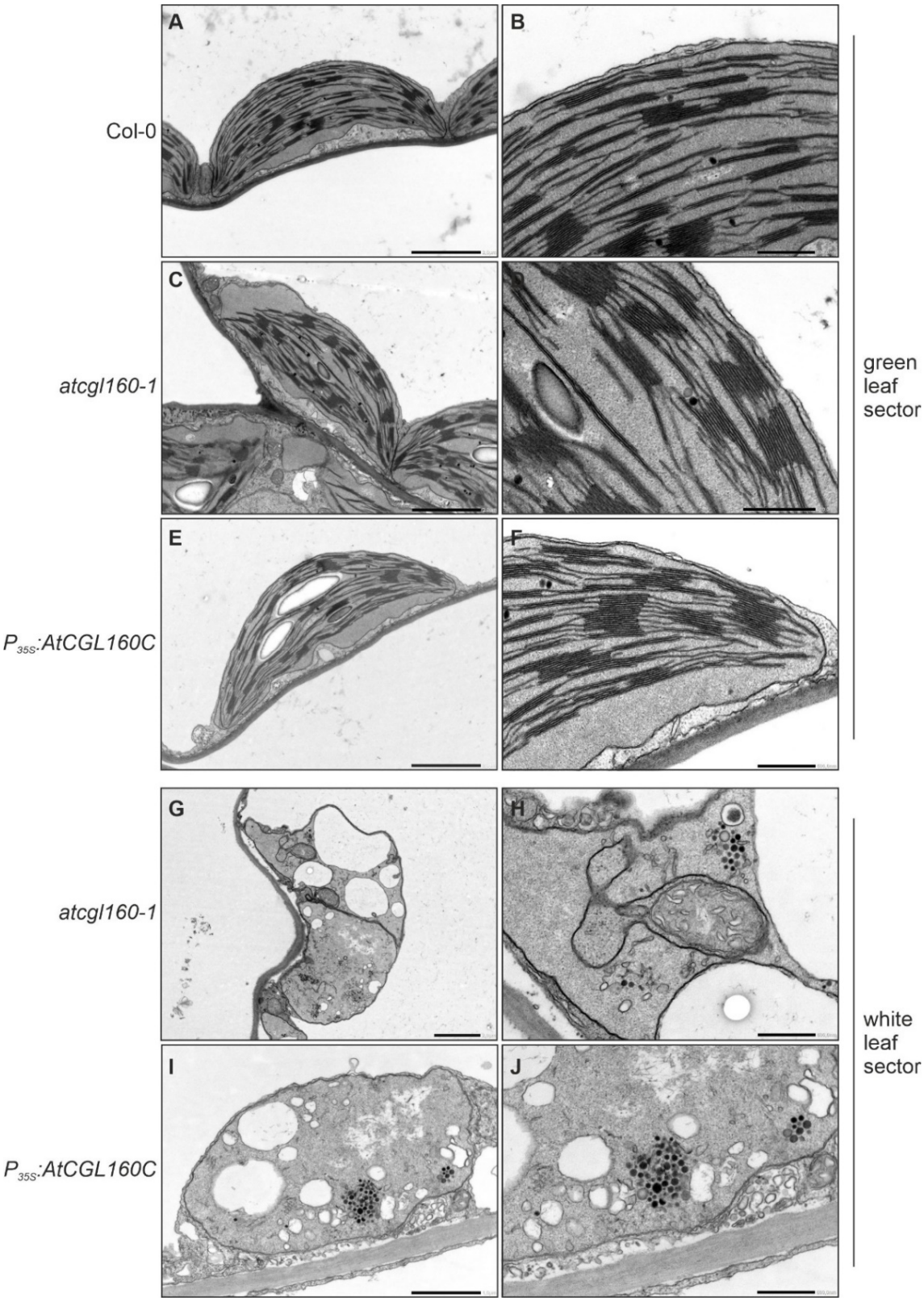

Figure 3. Plastid ultrastructure in white leaf sectors is altered in the absence of AtCGL160N under short-day growth conditions. Electron micrographs of sections of green leaves from Col-0 **(A, B)**, *atclg160-1* **(C, D)** and *P_{35S}:AtCGL160C* **(E, F)** plants. The ultrastructure of chloroplasts was further examined in sections of white leaves obtained from *atcgl160-1* **(G, H)** and *P_{35S}:AtCGL160C* **(I, J)** plants. The photos on the right show enlargements of the images on the left. The scale bar corresponds to 2 µm in **A**, **C**, **E**, and **G**, 1 µm in I and 0.5 µm in **B**, **D**, **F**, **H** and **J**.

To test whether disruption of AtCGL160N impairs photosynthesis and CF_1-CF_O activity, measurements of chlorophyll *a* fluorescence and electrochromic shift (ECS) were carried out on Col-0, *atcgl160-1*, *P_{35S}:AtCGL160, P_{35S}:AtCGL160N*, *P_{35S}:AtCGL160C* and *atcgld11-1* plants (Fig. 4A-C). As expected, the CF_1-CF_O assembly mutants *atcgl160-1* and *atcgld11-1* showed higher heat dissipation (indicated as non-photochemical quenching, NPQ) and increased proton-motive force (*pmf*), but lower proton conductivity (gH^+) through the thylakoid membrane compared to the wild-type control. *P_{35S}:AtCGL160* and *P_{35S}:AtCGL160N* plants displayed similar levels of NPQ, *pmf* and gH^+ to the wild type and the CF_1-CF_O assembly mutant *atcgld11-1*, respectively. Notably, photosynthetic parameters were only partially restored in *P_{35S}:AtCGL160C* lines.

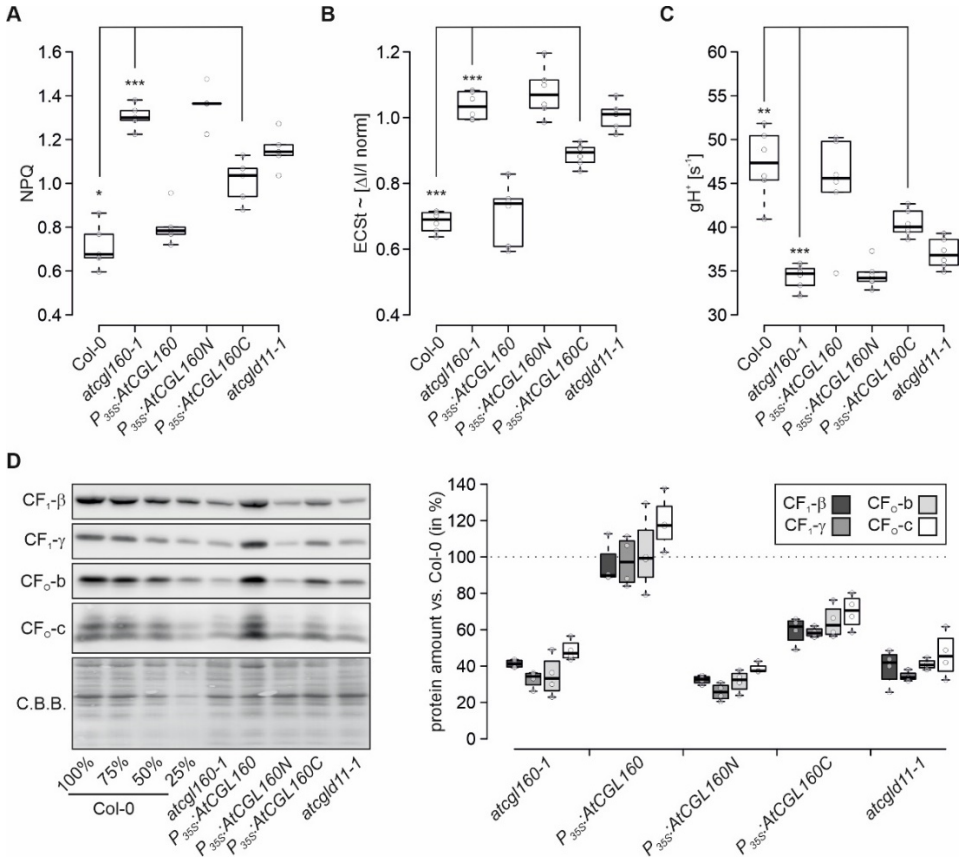

Figure 4. Lack of AtCGL160N perturbs photosynthesis and CF_1-CF_O integrity. **A**, Heat dissipation (non-photochemical quenching, NPQ) in Col-0, *atcgl160-1*, *P_{35S}:AtCGL160, P_{35S}:AtCGL160N*, *P_{35S}:AtCGL160C* and *atcgld11-1* plants grown under short-day conditions. NPQ values from five plants per genotype were determined 105 s after light induction (145 µmol photons m^{-2} s^{-1}) using an Imaging-PAM system (Walz). **B**, Dark-interval relaxation kinetics (DIRK) derived from ECS signals were recorded after 10 min of illumination from six individual plants grown under short-day conditions. Total amplitude of the P515 differential absorption signal was normalized to a single turnover flash 4 min after the ECS measurement. **C**, Proton conductivity of the thylakoid membrane was determined from ECS signal relaxation rates, which were fitted to a first-order decay function. Calculated rate constants were expressed as gH^+ [s^{-1}]. **D**, Steady-state levels of immunodetected CF_1-CF_O marker subunits. After fractionation of thylakoid proteins on SDS-PAGE and transfer to PVDF membranes, blots were probed with antibodies against CF_1-β, CF_1-γ, CF_O-b, and CF_O-c. Coomassie Brilliant Blue (C.B.B.) staining is shown as loading control. For quantification, signals from four technical replicates of each marker subunit were normalized to signals detected in Col-0 samples.

230 Horizontal lines represent the median, and boxes indicate the 25th and 75th percentiles.
231 Whiskers extend the interquartile range by 1.5×. The effect of the deletion of AtCGL160N on
232 photosynthetic parameters of *P_{35S}:AtCGL160C* plants shown in panels **A-C** was tested in
233 paired-sample t-tests (two-sided). Statistically significant differences are marked with asterisks
234 (**P*<0.05, ***P*<0.01, and ****P*<0.001).
235

236 To assess the integrity of the CF_1-CF_O complex in thylakoids, marker subunits were
237 immunodetected in *atcgl160-1*, *P_{35S}:AtCGL160, P_{35S}:AtCGL160N*, *P_{35S}:AtCGL160C* and
238 *atcgld11-1* plants, and quantified relative to Col-0 samples (Fig. 4D). Levels of CF_1-β, CF_1-γ,
239 CF_O-b and CF_O-c were restored to normal in *P_{35S}:AtCGL160*, but reduced to about 60-65% of
240 wild-type amounts in *P_{35S}:AtCGL160C* plants. Transformation with the *P_{35S}:AtCGL160N*
241 construct had no effect on CF_1-CF_O subunit levels in the *atcgl160-1* mutant.
242 Overall, overexpression of the Atp1/Unc1-like AtCGL160 domain alone (AtCGL160C) in the
243 *atcgl160-1* background only partially restored CF_1-CF_O amounts (Fig. 4D) and activity (Fig.
244 4C). Consequently, ΔpH-dependent quenching mechanisms (Fig. 4A) were more highly
245 activated, resulting in downregulation of photosynthesis (Fig. 4B) and growth impairment of
246 *P_{35S}:AtCGL160C* plants. We deduced from these results that AtCGL160N might also be
247 involved in CF_1-CF_O assembly at steps other than CF_O-c ring formation.
248

249 <u>Stromal accumulation of CF_1 in the absence of AtCGL160N</u>

250 To investigate the effects of deletion of AtCGL160N on CF_1-CF_O assembly, we performed
251 BN/SDS-PAGE (2D-PAGE) analysis on thylakoids isolated from *P_{35S}:AtCGL160* and
252 *P_{35S}:AtCGL160C* plants grown under short-day conditions. Consistent with the accumulation
253 of CF_1-CF_O marker subunits in Fig. 4D, CF_1-β, CF_O-b and CF_O-c levels were reduced in
254 *P_{35S}:AtCGL160C* compared to plants that overexpressed the full-length CDS of AtCGL160
255 (Fig. 5A). No accumulation of pre-complexes was observed, as amounts of free proteins, and
256 components of the c-ring, CF_1 and the holo-complex were reduced uniformly. To assess the
257 assembly status of the c-ring in more detail, we carried out 2D-PAGE with increased amounts
258 of *atcgl160-1* and *P_{35S}:AtCGL160C* thylakoids (Fig. 5B). C-ring levels were considerably higher
259 in *P_{35S}:AtCGL160C* than in the *atcgl160-1* mutant background. We also examined CF_1
260 accumulation in the stroma of Col-0, *P_{35S}:AtCGL160, P_{35S}:AtCGL160N*, *P_{35S}:AtCGL160C* and
261 *atcgld11-1* plants (Fig. 5C), since CF_1-CF_O assembly takes place in a modular fashion and
262 involves distinct thylakoid-integral and soluble intermediates. Strikingly, CF_1-β and CF_1-γ were
263 enriched about 10-fold in the stroma of *atcgl160-1*, *P_{35S}:AtCGL160N* and *P_{35S}:AtCGL160C*, but
264 were detected in close to wild-type levels in *P_{35S}:AtCGL160* and *atcgld11-1* plants. In-depth
265 2D-PAGE analysis of CF_1 intermediates in *atcgl160-1*, and comparison with results from the
266 co-migration database for photosynthetic organisms (PCom-DB, Takabayashi et al., 2017),
267 revealed that in *atcgl160-1* stromal CF_1-β and CF_1-γ were predominantly present in an $\alpha_3\beta_3\gamma\varepsilon$
268 complex that lacked subunit CF_1-δ (Supplemental Fig. S4).

We concluded that re-introduction of the transmembrane Atp1/Unc1-like domain of AtCGL160 restores c-ring formation, but leads to an overall reduction in CF_1-CF_O levels due to a defect in the attachment of CF_1 to a membrane-integral CF_O intermediate.

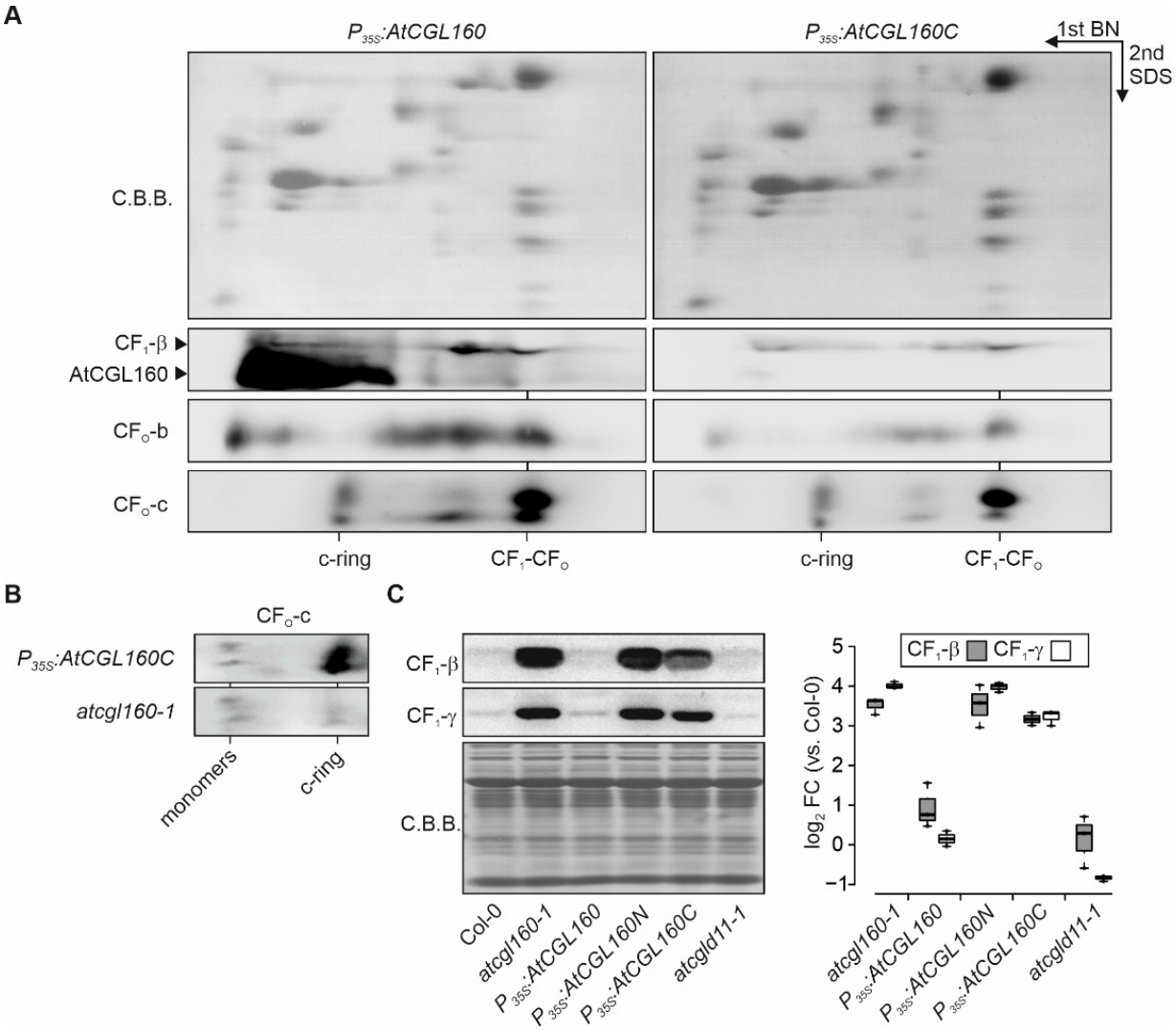

Figure 5. CF_1-CF_O assembly is perturbed in the absence of AtCGL160N. A, Thylakoid complexes from *P_{35S}:AtCGL160* and *P_{35S}:AtCGL160C* plants were solubilized with *n*-dodecyl *β*-D-maltoside (1% [w/v]) and further separated by Blue-Native (BN, 1st dimension) and SDS-PAGE (SDS, 2nd dimension). After protein transfer, PVDF membranes were probed with antibodies against CF_1-β, CF_O-b and CF_O-c, and CF_1-β blots were subsequently exposed to anti-AtCGL160 antibodies. Positions of the ATP synthase holo-complex (CF_1-CF_O) and the c-ring are indicated. Coomassie Brilliant Blue G-250 (C.B.B.) staining of PVDF membranes is shown as loading control. **B**, C-ring assembly in *atcgl160-1* and *P_{35S}:AtCGL160C* plants. Increased amounts of thylakoid complexes (corresponding to 120 µg total chlorophyll) were solubilized and fractionated by BN/SDS-PAGE. Blots were probed with an antibody against CF_O-c. Positions of free c-monomers and the assembled c-ring are indicated. **C**, CF_1-β and CF_1-γ enrichment in stromal extract, which was isolated from Col-0, *atcgl160-1*, *P_{35S}:AtCGL160, P_{35S}:AtCGL160N*, *P_{35S}:AtCGL160C* and *atcgld11-1* rosette leaves. Signals of three CF_1-β and CF_1-γ immunodetection assays were quantified and are shown on a logarithmic scale. Horizontal lines represent the median, boxes indicate the 25th and 75th percentiles and whiskers extend the interquartile range by a factor of 1.5×.

290 AtCGL160 interacts physically with CF_1-containing complexes

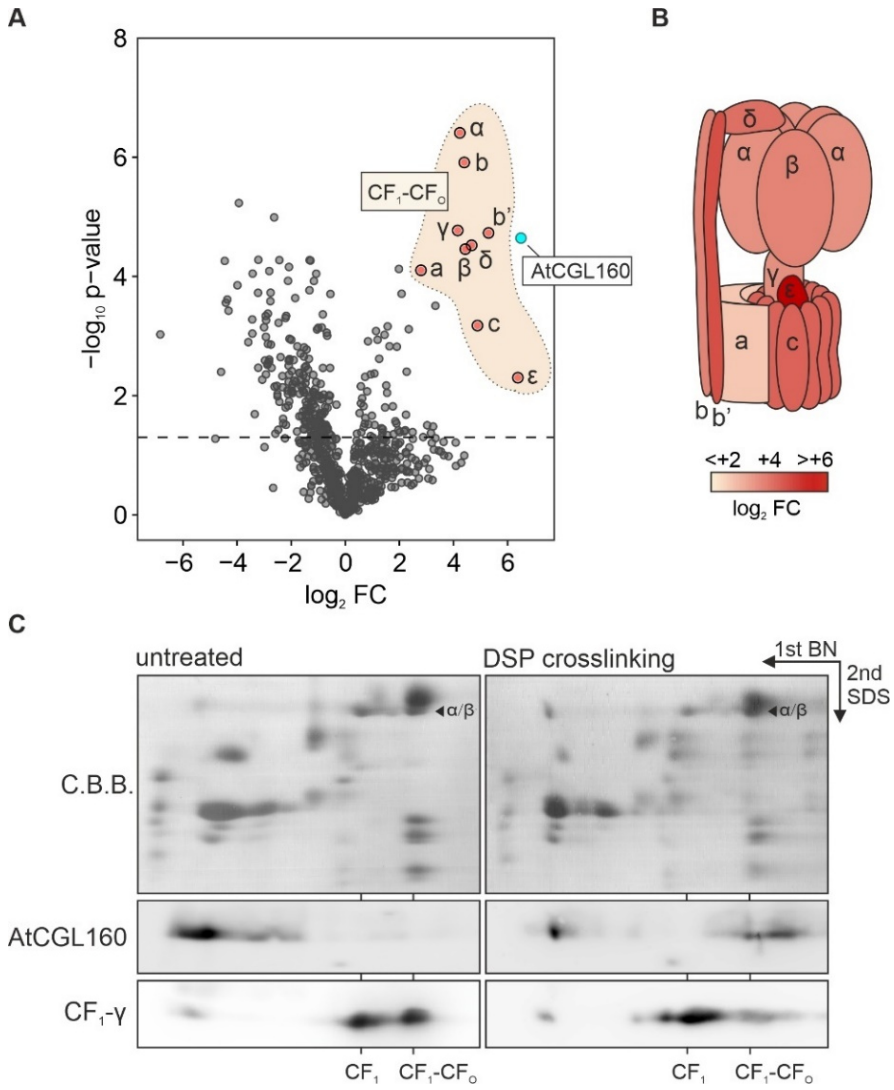

291

292 **Figure 6. AtCGL160 association with CF_1 subunits. A,** Co-immunoprecipitation analyses
293 were carried out with solubilized thylakoids isolated from *P_{35S}:AtCGL160,* while
294 *P_{35S}:AtCGL160C* plants served as the negative control. Co-immunoprecipitated proteins were
295 further subjected to tryptic digestion, and peptides were analyzed by liquid chromatography
296 coupled to mass spectrometry. Data for differentially enriched proteins are presented in a
297 volcano plot. The relative abundance (log_2 fold change [log_2 FC]) of proteins co-
298 immunoprecipitated from *P_{35S}:AtCGL160* samples is plotted against their statistically
299 significant enrichment as Benjamini-Hochberg corrected p-values (-log_{10} p-value). The dashed
300 line indicates a negative log_{10} p-value of 1.5, and was defined as the threshold for robust
301 reliability of differences in co-immunoprecipitation data. Blue and red dots highlight
302 quantification results for AtCGL160 and CF_1-CF_O subunits, respectively. **B**, Schematic
303 representation of differentially enriched subunits in a CF_1-CF_O cartoon. Relative amounts of
304 co-immunoprecipitated CF_1-CF_O subunits are shown in colors on a log_2 FC scale from white
305 (log_2 FC < 2) to red (log_2 FC > 6). Co-immunoprecipitation assays were carried out on three
306 independent biological replicates. **C,** Co-migration of AtCGL160 with CF_1-CF_O in crosslinking
307 experiments. Two-dimensional BN/SDS-PAGE analysis was used to compare untreated
308 thylakoid extracts of the WT (Col-0) with extracts that had been crosslinked with
309 dithiobis(succinimidyl propionate) (DSP). Blots of the second dimension were probed with
310 antibodies against AtCGL160 and CF_O-γ. The positions of CF_1-CF_O, the CF_1 intermediate, and
311 the free protein fraction are indicated based on the mobility of α/β on the C.B.B. stained gel.

312

313 To pinpoint the role of AtCGL160 in the recruitment of CF_1 to a membrane-integral CF_O
314 intermediate, protein interactions were assessed in co-immunoprecipitation (co-IP) assays
315 (Fig. 6B). Quantitative data for precipitated proteins were obtained by tryptic digestion and
316 subsequent peptide-fragment analysis using liquid chromatography coupled to mass
317 spectrometry. Since the commercially available AtCGL160 antibody (Agrisera AS12 1853)
318 displayed non-specific binding to either CF_1-α or CF_1-β (Supplemental Fig. 3), an AtCGL160
319 antibody with no significant cross-reactions to other thylakoid proteins was generated
320 (Supplemental Fig. 3). In the first step of antibody production, the N-terminal part of AtCGL160
321 ($AtCGL160_{29\text{-}206aa}$) was fused to the maltose-binding protein and injected into rabbits. In the
322 second step, antibodies specific for $AtCGL160_{29\text{-}206aa}$ were affinity-purified from rabbit antisera
323 using an immobilized fusion protein consisting of $AtCGL160_{29\text{-}206aa}$ and glutathione S-
324 transferase. As expected, when the resulting antibody fraction was tested in immunodetection
325 assays, it showed only one distinct signal in the WT sample, which was enriched in extracts of
326 *P_{35S}:AtCGL160*, but was absent in both the *atcgl160-1* mutant and in *P_{35S}:AtCGL160C* samples
327 (Supplemental Fig. 3).
328 Next, NP40-solubilized thylakoid proteins from *P_{35S}:AtCGL160* plants grown under short-day
329 conditions were chosen as co-IP input and pulled-down protein amounts were compared to
330 those recovered in co-IP experiments carried out on thylakoid protein extracts of
331 *P_{35S}:AtCGL160C*. Plants devoid of AtCGL160 were not considered for use as negative
332 controls, since the reduction in CF_1-CF_O levels observed in *atcgl160-1* (and *P_{35S}:AtCGL160N*)
333 (Fig. 4D) might lead to misinterpretation of differential co-IP experiments. As expected,
334 AtCGL160 was pulled down efficiently from *P_{35S}:AtCGL160C* extracts ($\log_2$ FC ~6.5).
335 Moreover, all CF_1-CF_O subunits were identified in co-IPs (Fig. 6A,B) with high differential
336 enrichment levels for the subunits α, β, γ, δ, ε, b, b' and c ($\log_2$ FC > 4.4). Subunit CF_O-a was
337 co-immunoprecipitated at lower levels ($\log_2$ FC ~2.8). The pull-down of CF_1 subunits was
338 confirmed by immunodetection assays of the two marker subunits CF_1-β and CF_1-γ, which
339 were only detectable in co-IP output fractions obtained from *P_{35S}:AtCGL160* samples
340 (Supplemental Fig. 5). Other known CF_1-CF_O assembly factors were not co-
341 immunoprecipitated (Supplemental Table 3), indicating that AtCGL160 is associated with a
342 late CF_1-CF_O assembly stage or the fully assembled complex from which other auxiliary factors
343 had already dissociated.
344 To confirm the association of AtCGL160 with CF_1-containing complexes, crosslinking
345 experiments were also carried out (Fig. 6C). To this end, thylakoid membranes of wild-type
346 plants were treated with the crosslinker dithiobis(succinimidyl propionate) (DSP), and
347 subsequently subjected to 2D-PAGE and immunodetection of AtCGL160 and CF_1-CF_O marker
348 subunits. In analyses with untreated thylakoid samples, AtCGL160 migrated predominantly in

349 the monomer fraction. After crosslinking, AtCGL160 could be detected at a molecular mass
350 range which corresponded to that of the CF_1-CF_O holo-complex.
351 In summary, co-IP of all CF_1-CF_O subunits with an AtCGL160-specific antibody, together with
352 the observation that AtCGL160 co-migrated with the CF_1-CF_O holo-complex after DSP cross-
353 linking, corroborates the involvement of AtCGL160 in the functional integration of CF_1 into the
354 holo-complex at a late step in CF_1-CF_O assembly.
355
356 <u>AtCGL160N interacts with CF_1-β in yeast two-hybrid assays</u>

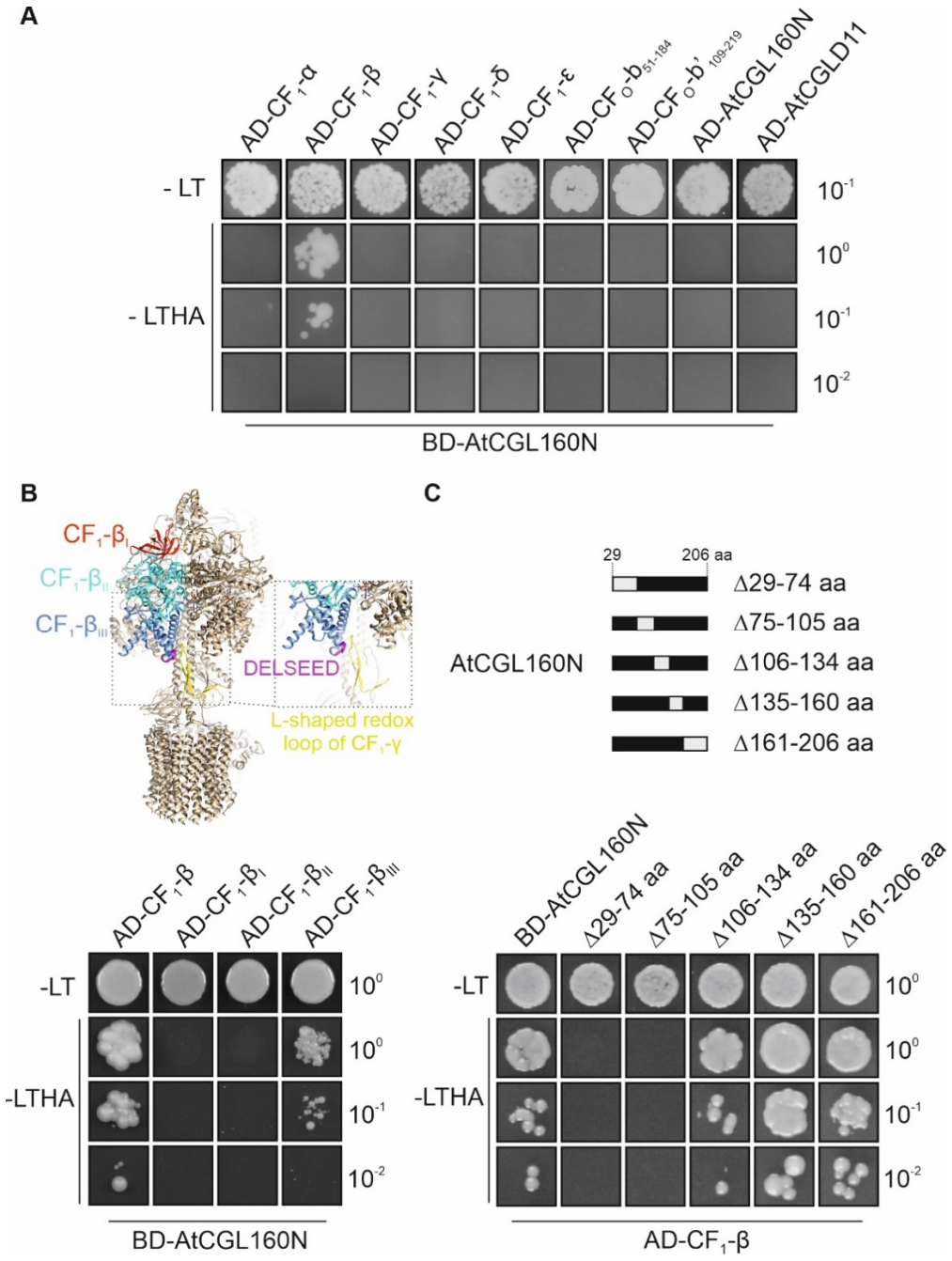

357

358 **Figure 7. AtCGL160N interaction studies in yeast two-hybrid assays. A**, Interactions of
359 AtCGL160 with CF_1-CF_O structural components exposed on the stromal side of thylakoids were
360 tested by transformation of a construct that fuses AtCGL160N to the GAL4 DNA-binding

361 domain (BD-AtCGL160). Cells were then co-transformed with constructs coding for GAL4
362 activation domain (AD) fused to CF_1-α, β, γ, δ, ε, CF_O-b_{51-184} or CF_O-$b'_{109-219}$, as well as
363 AtCGL160N or AtCGLD11. **B**, Interaction of AtCGL160N with structural domains of CF_1-β.
364 Yeast cells carrying a construct coding for BD-AtCGL160 were transformed with constructs
365 coding for AD-CF_1-β_I, AD-CF_1-β_{II}, and AD-CF_1-β_{III}. Structural domains of the CF_1-β are colored
366 in red (domain I), turquoise (domain II), and blue (domain III). The conserved DELSEED motif
367 is shown in purple, and the L-shaped redox loop of CF_1-γ in yellow. The atomic model of CF_1-
368 CF_O was obtained from the PDB database (ID: 6fkh, Hahn et al. (2018)) and formatted with
369 ChimeraX (Pettersen et al., 2021). **C,** Mapping of the AtCGL160N interaction site. Consecutive
370 regions (grey boxes) coding for segments of the soluble AtCGL160 domain were omitted from
371 the BD-AtCGL160N vector and co-transformed with AD-CF_1-β into competent yeast cells.
372 Transformations were verified by plating on permissive medium lacking Leu and Trp (-LT).
373 Interactions were then tested on selective medium (-Leu/-Trp/-His/-Ade, [-LTHA]) by plating
374 equal numbers of yeast cells in serial dilutions (10^0, 10^{-1}, and 10^{-2}).

375

376 Interactions between the stroma-oriented AtCGL160N domain and individual CF_1 subunits
377 were further examined by yeast two-hybrid experiments (Fig. 7). A construct coding for a
378 fusion of $AtCGL160N_{29-206aa}$ to the GAL4-binding domain (BD) was co-transformed into yeast
379 cells together with constructs coding for GAL4 activation domain (AD) fusions to all CF_1
380 subunits (α, β, γ, δ, ε). Moreover, BD-AtCGL160N interaction was tested with AD fusions to
381 the soluble parts of the stator subunits b and b', AtCGL160N, and CF_1 assembly factor
382 AtCGLD11. As a result, only yeast cells carrying constructs for AD-CF_1-β and BD-AtCGL160N
383 could grow on selective medium (Fig. 7A). To narrow down the CF_1-β interaction site, additional
384 AD fusion constructs were cloned that encoded three different CF_1-β subdomains (Fig. 7B)
385 defined in earlier studies (Groth and Pohl, 2001; Zhang et al., 2016). Domain I comprises a
386 thylakoid-distal β-barrel structure and interacts with CF_1-δ. Domain II harbors the catalytic site
387 involved in ATP generation or hydrolysis. The thylakoid-proximal domain III contains the
388 conserved "DELSEED" motif, which is required for CF_1-γ/ε-dependent regulation of ATP
389 hydrolysis and synthase activity (Kanazawa et al., 2017; Hahn et al., 2018). When tested on
390 restrictive medium, only cells harboring AD-CF_1-β_{III} together with BD-AtCGL160N could grow.
391 In a reciprocal approach, coding sequences of AtCGL160N were deleted successively from
392 the BD-AtCGL160N construct (Δ29-74, Δ75-105, Δ106-134, Δ135-160 and Δ161-206 aa) and
393 tested for AD-CF_1-β interaction in yeast cells (Fig. 7C). Only the Δ29-74 and Δ75-105 deletions
394 resulted in an absence of growth, while yeast strains with deletion constructs of Δ106-134,
395 Δ135-160 and Δ161-206 aa were able to proliferate on selective medium (Fig. 6B). Thus, the
396 interaction between AtCGL160 and CF_1 involves $AtCGL160_{29-105}$ and the thylakoid-proximal
397 domain of CF_1-β_{III}, while the phosphorylation hotspot identified in the protein segment 106-134
398 aa (Fig. 1A) is dispensable for the interaction.

399

400

401 **Discussion**

402

403 AtCGL160N recruits a stromal $\alpha_3\beta_3\gamma\varepsilon$ complex for late CF_1-CF_O assembly steps

404 Despite structural similarities and comparable subunit compositions, the number of known
405 assembly factors for ATP synthases is markedly higher in chloroplast than in bacterial systems
406 (reviewed in Zhang et al., 2020). Moreover, in plants the Atp1/UncI-related CGL160 assembly
407 factor has acquired an N-terminal domain that is specific for the green lineage. Thus, the
408 expanded molecular inventory for CF_1-CF_O assembly in chloroplasts might reflect the need for
409 tight post-translational control of CF_1-CF_O formation, since the complex plays a central role in
410 *pmf* utilization and regulation of photosynthesis (reviewed in Avenson et al., 2005). In this
411 context, an important finding of previous studies was that disruption of full-length AtCGL160
412 (Rühle et al., 2014; Fristedt et al., 2015) was more detrimental to levels of functional ATP
413 synthase than the loss of Atp1/UncI in bacteria (Gay, 1984; Liu et al., 2013). Furthermore, we
414 show here that expression of *P_{35S}:AtCGL160C* in plants that lack AtCGL160N only partially
415 restores CF_1-CF_O levels and activity (Fig. 4). These observations prompted us to investigate
416 the molecular function of the green-lineage-specific AtCGL160N in the CF_1-CF_O assembly
417 process in more detail.

418 Several lines of evidence suggest that the N-terminal domain of AtCGL160 recruits a stromal
419 CF_1 intermediate, while the C-terminal segment participates in c_{14}-ring assembly: (i)
420 AtCGL160N protrudes into the stroma, as deduced from protease protection assays (Fig. 1);
421 (ii) formation of the c_{14} ring is restored in the presence of AtCGL160C alone, but CF_1
422 accumulates strongly in the stroma in the absence of AtCGL160N (Fig. 5), (iii) CF_1 subunits
423 are differentially enriched in co-IP analyses performed with solubilized thylakoids isolated from
424 *P_{35S}:AtCGL160* plants (Fig. 6a,b), (iv) AtCGL160 co-migrates with a large complex after DSP-
425 mediated crosslinking (Fig. 6c) and (v) AtCGL160N interacts with CF_1-β in yeast two-hybrid
426 experiments (Fig. 7).

427 A role for AtCGL160 in the incorporation of CF_1 into the holocomplex was previously proposed
428 by Fristedt et al. (2015). This assumption was based on the observations that AtCGL160 co-
429 migrated with CF_1 subcomplexes in BN/SDS-PAGE analyses and could be cross-linked to CF_1
430 subunits in wild-type protein samples. However, we detected AtCGL160 predominantly in the
431 monomer fraction in untreated thylakoid preparations in this study (Fig. 6C), as well as in
432 previous work (Rühle et al., 2014) – and co-migration of AtCGL160 with high-molecular-mass
433 complexes was only observed after thylakoid proteins had been crosslinked with DSP (Fig.
434 6C). Furthermore, the commercially available AtCGL160 antibody (AS12 1853, Agrisera)
435 employed in the study of Fristedt et al. (2015) was found here to cross-react strongly with CF_1-
436 α or CF_1-β (Supplemental Fig. 3), which complicates the interpretation of one-dimensional co-
437 migration and crosslinking experiments in the absence of appropriate controls. Therefore, a

438 new antibody was generated that does not cross-react with CF_1-CF_O subunits and thus
439 provides a reliable means of probing the molecular interactions of AtCGL160 (Supplemental
440 Fig. 3).
441 Besides CGL160, ALB4 – a member of the bacterial ALB3/Oxa1/YidC protein insertase family
442 – was previously proposed to participate in the linkage of a CF_1 to a CF_O assembly module
443 (Benz et al., 2009). Another study provided evidence that ALB4 and its paralog ALB3 physically
444 interact with each other, and show significant functional overlap in the membrane insertion of
445 subunits of the Cyt b_6f complex (Trosch et al., 2015). Moreover, alleles of *ALB4* (*STIC1*) have
446 been identified as suppressors of the chloroplast protein import mutant *tic40* (Bedard et al.,
447 2017), and ALB4/STIC1 and STIC2 were shown to act together in thylakoid protein targeting
448 in a pathway that also involves cpSRP54 and cpFtsY. In our study, we did not identify
449 ALB4/STIC1 in co-IP experiments with anti-AtCGL160 antibodies (Fig. 6, Supplemental Table
450 S1) and amounts of thylakoid-associated CF_1-β in *atalb4-1* mutants (SALK_136199C) grown
451 under short-day conditions were unaltered (Supplemental Fig. S6). Thus, ALB4/STIC1 does
452 not act in concert with CGL160 in late stages of CF_1-CF_O assembly, but serves as a general
453 thylakoid protein biogenesis factor involved in folding or assembly of a specific subset of
454 transmembrane proteins (Bedard et al., 2017).

455

456 <u>AtCGL160 is critical for chloroplast development in the dark</u>
457 It has long been thought that the hydrolytic activity of CF_1-CF_O needs to be inactivated in the
458 dark to prevent futile ATP depletion (Ort and Oxborough, 1992). However, analysis of the
459 constitutively redox-activated γ-subunit mutant *gamera*, in which a 'dark *pmf*' is maintained,
460 revealed increased stability of photosynthetic complexes upon prolonged darkness,
461 suggesting that a certain degree of ATPase activity may be beneficial during the night
462 (Kohzuma et al., 2017). Concomitantly, several processes have been proposed to depend on
463 the maintenance of a dark *pmf*. These include thylakoid protein transport via the Tat- and Sec-
464 dependent pathways, modulation of protease activity and ion homeostasis in the chloroplast.
465 In this regard, a remarkable influence of AtCGL160 disruption on leaf variegation (Fig. 2) and
466 chloroplast development (Fig. 3) was observed exclusively under short-day conditions.
467 Surprisingly, this phenotype was not detectable in *atcgld11-1* plants with a defect in CF_1
468 assembly and reduced amounts of CF_1-CF_O comparable to those in *atcgl160-1* (Fig. 4D).
469 However, the leaf phenotype correlated with the accumulation of a CF_1 intermediate in the
470 stroma (Fig. 5C). Thus, AtCGL160-mediated CF_1 recruitment might also be critical in
471 preserving the dark *pmf* at night. Alternatively, stroma-enriched CF_1 complexes (Fig. 5C) could
472 alter the chloroplast ATP/ADP ratio by excessive hydrolytic activity, and disturb ATP-
473 dependent nocturnal processes that ultimately lead to premature chloroplast degradation (Fig.
474 3).

475

476 AtCGL160 is a central CF_1-CF_O assembly factor with multiple functions

477 Assembly of membrane-embedded ATP synthase modules and their subsequent association
478 with F_1 subcomplexes are critical steps in bacterial and organellar ATP synthase biogenesis,
479 as premature formation of the proton-translocating channel between the c-ring and the a-
480 subunit (equivalent to the ATP9 ring and the ATP6 subunit in mitochondria) can lead to
481 uncontrolled dissipation of the *pmf* (Birkenhäger et al., 1999; Franklin et al., 2004), and only
482 efficient integration of F_1 triggers ATP production. In this context, molecular aspects of the
483 assembly processes were recently elucidated for bacterial (reviewed in Deckers-Hebestreit,
484 2013), as well as yeast and human mitochondrial ATP synthases (reviewed in Song et al.,
485 2018). One significant outcome was that, while ATP synthase assembly pathways and the
486 repertoire of auxiliary factors differ among these systems, formation of the proton-translocating
487 unit during the final assembly steps is common to all of them.

488 Intriguingly, our data revealed a dual involvement of AtCGL160 in CF_1-CF_O assembly, namely
489 in c-ring formation and the recruitment of a CF_1 intermediate. In fact, these two events were
490 suggested to proceed sequentially in the assembly of bacterial ATP synthases (Deckers-
491 Hebestreit, 2013). Since an *E. coli* strain lacking subunit δ accumulates a $c_{10}\alpha_3\beta_3\gamma\varepsilon$
492 subcomplex, it is assumed that cytoplasmic F_1 first binds to the c_{10} ring, and $c_{10}\alpha_3\beta_3\gamma\varepsilon$
493 associates with the ab_2 module in a δ-dependent manner in the final assembly step (Hilbers et
494 al., 2013). By analogy with the bacterial assembly pathway, AtCGL160 may facilitate the
495 integration of a stator assembly module into the holo-complex. Indeed, the interaction of
496 AtCGL160C with CF_O-b has been demonstrated in split-ubiquitin assays (Rühle et al., 2014).
497 Moreover, CF_O-a was less highly enriched in co-IP analyses than other CF_1-CF_O subunits (Fig.
498 6A, B), which might argue for the release of AtCGL160 after functional incorporation of CF_O-a
499 in the final steps of CF_1-CF_O assembly. In this scenario, AtCGL160 could act as a placeholder
500 to prevent the premature formation of proton-translocating intermediates. A similar function
501 has been described for the INA complex in yeast mitochondria, which binds to the c-ring, but
502 also to a distinct assembly intermediate consisting of ATP6, ATP8, ATP10, ATP23, peripheral
503 stalk subunits and the F_1 domain (Naumenko et al., 2017). This ensures that the c-ring and
504 subunit ATP6 are assembled into the proton-conducting unit in a controlled manner. However,
505 due to a generally low turnover rate of CF_1-CF_O assembly (reviewed in Schöttler et al., 2014)
506 and inefficient detection of distinct thylakoid-integral intermediates, a robust CF_O assembly
507 map is still lacking, and 'true' stator-containing assembly modules have not been described so
508 far.

509 Nevertheless, a straightforward assembly mechanism for the recruitment of CF_1 can be derived
510 from our study. After AtCGL160-assisted ring formation (Rühle et al., 2014), the stromally
511 oriented AtCGL160N (Fig. 1) binds to a CF_1 intermediate consisting of $\alpha_3\beta_3\gamma\varepsilon$ but not subunit

δ (Fig. 5C, Supplemental Fig. S4). Recruitment is mediated through interaction of AtCGL160$_{29-105}$ with subunit CF$_1$-β; thus, the phosphorylatable AtCGL160 segment is dispensable for the interaction (Fig. 7). Since AtCGL160 can be cross-linked to high-molecular-mass complexes that are larger than CF$_1$ (Fig. 6C), AtCGL160 might remain attached to a putative $c_{14}\alpha_3\beta_3\gamma\varepsilon$ or $bb'c_{14}\alpha_3\beta_3\gamma\varepsilon$ intermediate. Its release could then be triggered by the incorporation of subunit CF$_O$-a or CF$_1$-δ in the final assembly steps.

At this stage, we cannot rule out the possibility that AtCGL160N might have regulatory functions beyond CF$_1$ recruitment, as it interacts with the thylakoid-proximal domain III of CF$_1$-β, which contains the conserved DELSEED motif (Fig. 7B). Several regulatory mechanisms have been elucidated in which the subunit β and the DELSEED motif are implicated. For instance, the autoinhibitory subunit ε interacts with the DELSEED motif in bacteria (Tanigawara et al., 2012; Sobti et al., 2016), whereas in bovine (Cabezon et al., 2003) and yeast mitochondria (Robinson et al., 2013), the small protein IF$_1$ inhibits ATPase activity by binding at the α/β interface. In plants, a regulatory mechanism controls CF$_1$-CF$_O$ activity involving also the DELSEED and an L-shaped, two β-hairpin containing motif with two conserved redox-sensitive cysteines in the CF$_1$-γ subunit (Hahn et al., 2018). By analogy with the role of IF$_1$, which was shown to inhibit ATPase activity during the assembly of human mitochondrial ATP synthases (He et al., 2018), AtCGL160N may regulate ATPase activity during CF$_1$-CF$_O$ assembly via an as yet unknown mechanism.

532 **Methods**

533

534 Bioinformatics Sources

535 Protein and gene sequences were downloaded from the Arabidopsis Information Resource
536 server (TAIR; http://www.arabidopsis.org), Phytozome
537 (https://phytozome.jgi.doe.gov/pz/portal.html) and the National Center for Biotechnology
538 Information server (NCBI; http://www.ncbi.nlm.nih.gov/). Transit peptides were predicted by
539 ChloroP (http://www.cbs.dtu.dk/services/ChloroP/) (Emanuelsson et al., 1999). Structural data
540 was obtained from the PDB homepage (https://www.rcsb.org/) and processed with ChimeraX
541 (https://www.cgl.ucsf.edu/chimerax/) (Pettersen et al., 2021). Multiple sequence alignments
542 were generated with the CLC workbench software (v8.1) and protein features were visualized
543 with Protter (https://wlab.ethz.ch/protter/start/) (Omasits et al., 2014). Co-migration of stromal
544 proteins was examined with the online tool PCom-DB
545 (http://pcomdb.lowtem.hokudai.ac.jp/proteins/top) (Takabayashi et al., 2017). Boxplots were
546 drawn with BoxPlotR (http://shiny.chemgrid.org/boxplotr/) (Spitzer et al., 2014).

547

548 Plant Material and Growth Conditions

549 T-DNA lines for *atcgl160-1 (*SALK_057229, Col-0 background*)*, *atcgld11-1* (SALK_019326C*,*
550 Col-0 background) and *atalb4-1* (SALK_136199C) were obtained from the SALK collection
551 (Alonso et al., 2003). Plants were grown on potting soil (A210, Stender) under controlled
552 greenhouse conditions (70-90 µmol photons m^{-2} s^{-1}, 16/8 h light/dark cycles), or in climate
553 chambers on an 8h light/16h dark cycle for biochemical and physiological analyses. Fertilizer
554 was added to plants grown under greenhouse conditions according to the manufacturer's
555 recommendations (Osmocote Plus; 15% nitrogen [w/v], 11% [w/v] P_2O_5, 13% [w/v] K_2O, and
556 2% [w/v] MgO; Scotts Germany). For domain-specific complementation assays, either the
557 complete coding region of *AtCGL160* (*P_{35S}:AtCGL160*) or parts of the CDS corresponding to
558 amino acids 1-206 (*P_{35S}:AtCGL160N*) and 207-350 (*P_{35S}:AtCGL160C*) were cloned into the
559 binary Gateway vector pB2GW7 (Karimi et al., 2002), placing the genes under control of the
560 35S CaMV promoter. The transit peptide coding sequence (for amino acids 1-46) was fused
561 to the *AtCGL160C* CDS in the case of the *P_{35S}:AtCGL160C* vector. The constructs were first
562 transformed into *Agrobacterium tumefaciens* strain GV3101, and then into *atcgl160-1* plants
563 by the floral-dip method (Clough and Bent, 1998). T1 plants were selected by screening for
564 Basta resistance. Basta positives were screened for equal amounts of the *AtCGL160* transcript
565 by RNA gel-blot hybridization as described below.

566

567 Chl *a* Fluorescence Measurements

568 *In vivo* Chl a fluorescence of whole plants was measured using an imaging Chl fluorometer
569 (Imaging PAM, Walz, Effeltrich, Germany). Plants were dark-adapted for 20 min and exposed
570 to a pulsed, blue measuring beam (4 Hz, intensity 3, gain 3, damping 2; F_O) and a saturating
571 light flash (intensity 10) to calculate F_V/F_M. If not indicated otherwise, transient NPQ induction
572 was measured at 145 µmol photons m^{-2} s^{-1}.

573

574 ECS Measurements

575 ECS measurements were performed using the Dual-PAM-100 (Walz, Effeltrich, Germany)
576 equipped with a P515/535 emitter-detector module (Schreiber and Klughammer, 2008). The
577 measurement was carried out at 23°C under ambient CO_2 conditions. Plants grown in short-
578 day conditions for four weeks were light-adapted, and detached leaves were illuminated for at
579 least 10 min with 129 µmol photons m^{-2} s^{-1} red light. After illumination, dark-interval relaxation
580 kinetics (DIRK) were measured in the ms to s range. Values for *pmf* (ECSt), and proton
581 conductivity (gH^+) were calculated as described (Cruz et al., 2001; Schreiber and Klughammer,
582 2008). Briefly, the maximum amplitude of the inverse electrochromic band-shift kinetic was
583 measured in the second range, and normalized to a single saturating P515 pulse measured
584 after 4 minutes of dark incubation. For proton conductivity, electrochromic band-shift kinetics
585 were recorded in the millisecond range for 5 consecutive periods of 2 sec, separated by dark
586 intervals of 30 sec. The combined signals were fitted to a single exponential decay function
587 and the reciprocal value of the lifetime was used to estimate the proton conductivity (Kanazawa
588 and Kramer, 2002).

589

590 AtCGL160 Antibody Generation

591 Rabbit antibodies were generated against AtCGL160 that had been heterologously expressed
592 in *Escherichia coli*, and then purified. To this end, the coding sequence corresponding to
593 $AtCGL160_{29-206}$ was cloned into the pMal-c5x vector (New England Biolabs) and purified on
594 amylose columns (New England Biolabs) according to the manufacturer's instructions. The
595 protein was injected into rabbits for antibody production (Pineda, Berlin, Germany). To reduce
596 epitope cross-reactions, the antiserum was purified on a column crosslinked with
597 heterologously expressed $AtCGL160_{29-206}$ fused to the glutathione-S-transferase (GST) tag.
598 Purified antibody was employed at a dilution of 1:1000. Signals were detected by enhanced
599 chemiluminescence (Pierce™ ECL Western Blotting Substrate, Thermo Scientific) using an
600 ECL reader system (Fusion FX7; PeqLab, Erlangen, Germany).

601

602 Nucleic Acid Analysis

603 Total RNA from snap-frozen leaves was extracted with the RNeasy Plant Mini Kit (Qiagen)
604 according to the supplier's instructions. Samples equivalent to 8 or 20 µg total RNA were
605 fractionated by electrophoresis in formaldehyde-containing agarose gels (1.2%), blotted onto
606 nylon membranes (Hybond-N+, Amersham Bioscience) and fixed by UV radiation
607 (Stratalinker® UV Crosslinker 1800). To control for equal loading, abundant RNAs on nylon
608 membranes were stained with methylene blue solution (0.02% [w/v] methylene blue, 0.3 M
609 sodium acetate pH 5.5). To detect gene-specific transcripts, DNA fragments amplified from
610 cDNA were labelled with radioactive [α-^{32}P]dCTP and subsequently used as probes in
611 hybridization experiments (see Supplemental Table S2 for primer information). Signals were
612 detected with the Typhoon Phosphor Imager System (GE Healthcare).

613

614 Protein Analysis

615 Leaves from 4-week-old plants grown under short-day conditions were harvested shortly after
616 the onset of the light period, and thylakoid membrane-enriched samples were isolated
617 according to Rühle et al. (2014). Crosslinking of thylakoids was performed by incubation with
618 2.5 mM dithiobis succinimidyl propionate (DSP, Thermo Scientific). After incubation for 20 min
619 on ice, crosslinking was quenched with 60 mM Tris/HCl (pH 7.5). Chl concentrations were
620 determined as described in Porra et al. (1989). For immunotitrations, thylakoid membrane
621 pellets were resuspended in loading buffer (100 mM Tris-HCl pH 6.8, 50 mM dithiothreitol
622 [DTT], 8% [w/v] SDS, 24% [w/v] glycerol and 0.02% [w/v] bromophenol blue). Denaturation for
623 5 min at 70°C and protein fractionation on Tricine-SDS-PAGE gels (10% gels supplemented
624 with 4M Urea) was carried out according to Schägger (2006). Immunodetections were
625 performed as described below. Sample preparation for BN-PAGE was performed with freshly
626 prepared thylakoids as described in Peng et al. (2008). First, membranes were washed twice
627 in wash buffer (20% glycerol, 25 mM BisTris/HCl pH 7.0). Then, samples were treated with
628 wash buffer containing 1% (w/v) n-dodecyl β-D-maltoside and adjusted to 1 ml mg^{-1} Chl for 10
629 min on ice. After centrifugation (16,000*g*, 20 min, 4°C), supernatants were supplemented with
630 1/10 volume of BN sample buffer (100 mM BisTris/HCl pH 7.0, 750 mM ε-aminocaproic acid,
631 5% [w/v] Coomassie G-250). BN-PAGE gels (4-12% gradient) were prepared as described in
632 Schägger et al. (1994). Solubilized samples corresponding to 60 µg Chl were loaded per lane
633 and gels were run at 4°C overnight. To separate complexes into their subunits, BN-PAGE
634 strips were treated with denaturing buffer (0.2 M Na_2CO_3, 5% [w/v] SDS, 50 mM DTT) for 30
635 min at room temperature and loaded on Tricine-SDS-PAGE gels. Gels were subsequently

636 subjected to immunoblot analysis with antibodies against CF_1-CF_O subunits and AtCGL160,
637 as described below.
638 For analysis of the stromal CF_1 intermediate, intact chloroplasts from 4-week-old plants were
639 isolated according to Rühle et al. (2021). After lysis in 25 mM HEPES/KOH (pH 7.5) containing
640 5 mM $MgCl_2$ for 30 min on ice, the stromal fraction was separated from membranes by
641 centrifugation at 35,000*g* for 30 min (4 °C). Protein concentration was measured using the
642 Bradford Protein Assay (Bio-Rad). Stromal BN analysis was performed according to Reiter et
643 al. (2020). In brief, chloroplast-enriched pellets were resuspended in BN washing buffer and
644 mechanically disrupted by passage through an 0.45-mm syringe. The stromal fraction was
645 separated from membranes by centrifugation at 35,000*g* for 30 min (at 4°C). 100 µg of total
646 soluble protein was mixed with 1/10 volume of BN sample buffer before fractionation in the first
647 dimension as described above.
648

649 Immunoblot Analyses

650 Proteins fractionated by gel electrophoresis were transferred to polyvinylidene difluoride
651 membranes (PVDF) (Immobilon®-P, Millipore) using a semi-dry blotting system (Biorad) as
652 described in the supplier's instructions. After blocking with TBST (10 mM Tris pH 8.0, 150 mM
653 NaCl and 0.1% [v/v] Tween-20) supplemented with 3% (w/v) skim milk powder, the membranes
654 were incubated with antibodies at 4°C overnight. Antibodies used in this study were obtained
655 from Agrisera (CF_1-β: AS05 085, 1:5000; CF_1-γ: AS08 312, 1:5000; CF_O-b: AS10 1604, 1:5000;
656 CF_O-c: AS09 591, 1:3000; and AtCGL160: AS12 1853, 1:1000).

657

658 Yeast-two-Hybrid Experiments

659 Yeast two-hybrid assays were carried out using the Matchmaker Two-Hybrid System Kit
660 (Clontech). The *AtCGL160* CDS without the signal peptide (see Supplemental Table S2 for
661 primer information) was cloned into the bait vector pGBKT7 (BD-AtCGL160), whereas the
662 coding sequences of CF_1-α, -β, -γ, -δ, -ε, the soluble domains of CF_O-b (51-184 aa) and b'
663 (109-219 aa), AtCGL160 and the CF_1 assembly factor AtCGLD11 were cloned into the prey
664 vector pGADT7 (named AD-CF_1-α, AD-CF_1-β, AD-CF_1-γ, AD-CF_1-δ, AD-CF_1-ε, AD-CF_O-b, AD-
665 CF_O-b', AD-AtCGL160 and AD-AtCGLD11). As in the case of AtCGL160, signal peptide
666 sequences were omitted from the nucleus-encoded subunits CF_1-γ, CF_1-δ, CF_O-b' and
667 AtCGLD11. For binding-domain analysis of CF_1-β, the respective CDS was sub-divided into
668 three parts, according to Groth and Pohl (2001) and cloned into pGADT7. In the case of
669 AtCGL160N binding-site analysis, sequences coding for 29-74, 75-105, 106-134, 135-160 and
670 161-206 aa were deleted from the BD-AtCGL160 vector using a site-directed mutagenesis kit

671 (NEB). Primers are listed in Supplemental Table S2. Bait and prey vectors were co-
672 transformed into AH109 yeast strains (Clontech) following manufacturer's instructions. Co-
673 transformants were selected on synthetic dropout (SD) medium (Clontech) lacking leucine and
674 tryptophan (-LT). In order to identify protein interactions, double transformants were grown on
675 SD medium lacking leucine, tryptophan, histidine, and adenine (-LTHA).
676
677 Co-immunoprecipitation

678 Freshly extracted thylakoids corresponding to ~10 mg chlorophyll were resuspended in 500 µl
679 extraction buffer (50 mM Tris/HCl pH 7.5, 150 mM NaCl, 1 mM $MgCl_2$, 5% [w/v] glycerol, 1%
680 [v/v] Nonidet P40 [NP40], 0.2 mM phenylmethylsulfonyl fluoride [PMSF]) and solubilized for 30
681 min on ice. After centrifugation at 35,000*g* for 30 min and 4°C, the supernatant was added to
682 20 µl Dynabeads (Thermo Scientific), equilibrated with equilibration buffer (50 mM Tris/HCl pH
683 7.5, 150 mM NaCl, 5% [w/v] glycerol, 0.05% [v/v] NP40) and labelled with AtCGL160 antibody
684 according to the manufacturer's instructions. The suspension was incubated with rotation for
685 3 h at 4°C, washed three times with equilibration buffer, and twice with the same buffer but
686 omitting NP40. Proteins were eluted with 100 µl 0.1 M glycine pH 2.0 for 10 min and neutralized
687 with 100 µl 0.1 M ammonium bicarbonate. After treatment with 10 µl of 45 mM DTT and 10 µl
688 of 0.1 M iodoacetamide, samples were digested with 1.5 µg of trypsin at 37°C overnight.
689 Peptides were desalted with home-made C18 stage tips (Rappsilber et al., 2003), vacuum-
690 dried to near dryness and stored at –80°C. LC MS/MS run and data analysis were performed
691 as described in Reiter et al. (2020).
692

693 **Author Contributions**

694 B.R. and T.R. designed research. B.R., L.R., G.M., S.G. and T.R. carried out experiments.
695 B.R., D.L. and T.R. prepared the article. T.R. supervised the whole study.
696

697 **Acknowledgments**

698 We thank Tim Scheibenbogen, Michael Berger and Tanja Neufeld for technical assistance with
699 Yeast-two-hybrid experiments, Tim Dreißig for technical assistance with heterologous
700 expression of AtCGL160N, and Paul Hardy for critical comments on the manuscript.

701

702 **Funding information**

703 This work was funded by the German Science Foundation (DFG, Research Unit FOR2092,
704 project number 239484859, grant RU 1945/2-1).

705 ## References

706 **Alonso, J.M., Stepanova, A.N., Leisse, T.J., Kim, C.J., Chen, H., Shinn, P., Stevenson,**
707 **D.K., Zimmerman, J., Barajas, P., Cheuk, R., Gadrinab, C., Heller, C., Jeske, A.,**
708 **Koesema, E., Meyers, C.C., Parker, H., Prednis, L., Ansari, Y., Choy, N., Deen,**
709 **H., Geralt, M., Hazari, N., Hom, E., Karnes, M., Mulholland, C., Ndubaku, R.,**
710 **Schmidt, I., Guzman, P., Aguilar-Henonin, L., Schmid, M., Weigel, D., Carter,**
711 **D.E., Marchand, T., Risseeuw, E., Brogden, D., Zeko, A., Crosby, W.L., Berry,**
712 **C.C., and Ecker, J.R.** (2003). Genome-wide insertional mutagenesis of Arabidopsis
713 thaliana. Science (New York, N.Y.) **301,** 653-657.

714 **Avenson, T.J., Kanazawa, A., Cruz, J.A., Takizawa, K., Ettinger, W.E., and Kramer, D.M.**
715 (2005). Integrating the proton circuit into photosynthesis: progress and challenges.
716 Plant Cell and Environment **28,** 97-109.

717 **Bedard, J., Trosch, R., Wu, F.J., Ling, Q.H., Flores-Perez, U., Topel, M., Nawaz, F., and**
718 **Jarvisa, P.** (2017). Suppressors of the Chloroplast Protein Import Mutant tic40
719 Reveal a Genetic Link between Protein Import and Thylakoid Biogenesis. Plant Cell
720 **29,** 1726-+.

721 **Benz, M., Bals, T., Gügel, I.L., Piotrowski, M., Kuhn, A., Schünemann, D., Soll, J., and**
722 **Ankele, E.** (2009). Alb4 of Arabidopsis promotes assembly and stabilization of a non
723 chlorophyll-binding photosynthetic complex, the CF1CF0-ATP synthase. Molecular
724 plant **2,** 1410-1424.

725 **Birkenhäger, R., Greie, J.C., Altendorf, K., and Deckers-Hebestreit, G.** (1999). F0
726 complex of the Escherichia coli ATP synthase. Not all monomers of the subunit c
727 oligomer are involved in F1 interaction. European journal of biochemistry / FEBS **264,**
728 385-396.

729 **Cabezon, E., Montgomery, M.G., Leslie, A.G., and Walker, J.E.** (2003). The structure of
730 bovine F1-ATPase in complex with its regulatory protein IF1. Nat Struct Biol **10,** 744-
731 750.

732 **Chen, G.G., and Jagendorf, a.T.** (1994). Chloroplast molecular chaperone-assisted
733 refolding and reconstitution of an active multisubunit coupling factor CF1 core.
734 Proceedings of the National Academy of Sciences of the United States of America
735 **91,** 11497-11501.

736 **Clough, S.J., and Bent, A.F.** (1998). Floral dip: a simplified method for Agrobacterium-
737 mediated transformation of Arabidopsis thaliana. Plant J **16,** 735-743.

738 **Cruz, J.A., Sacksteder, C.A., Kanazawa, A., and Kramer, D.M.** (2001). Contribution of
739 electric field (Delta psi) to steady-state transthylakoid proton motive force (pmf) in
740 vitro and in vivo. control of pmf parsing into Delta psi and Delta pH by ionic strength.
741 Biochemistry **40,** 1226-1237.

742 **Daum, B., Nicastro, D., Austin, J., McIntosh, J.R., and Kühlbrandt, W.** (2010).
743 Arrangement of photosystem II and ATP synthase in chloroplast membranes of
744 spinach and pea. The Plant cell **22,** 1299-1312.
745 **Deckers-Hebestreit, G.** (2013). Assembly of the Escherichia coli FoF1 ATP synthase
746 involves distinct subcomplex formation. Biochemical Society transactions **41,** 1288-
747 1293.
748 **Eberhard, S., Loiselay, C., Drapier, D., Bujaldon, S., Girard-Bascou, J., Kuras, R.,**
749 **Choquet, Y., and Wollman, F.-A.** (2011). Dual functions of the nucleus-encoded
750 factor TDA1 in trapping and translation activation of atpA transcripts in
751 Chlamydomonas reinhardtii chloroplasts. The Plant journal : for cell and molecular
752 biology **67,** 1055-1066.
753 **Emanuelsson, O., Nielsen, H., and von Heijne, G.** (1999). ChloroP, a neural network-
754 based method for predicting chloroplast transit peptides and their cleavage sites.
755 Protein Science : A Publication of the Protein Society **8,** 978-984.
756 **Franklin, M.J., Brusilow, W.S.a., and Woodbury, D.J.** (2004). Determination of proton flux
757 and conductance at pH 6.8 through single FO sectors from Escherichia coli.
758 Biophysical journal **87,** 3594-3599.
759 **Fristedt, R., Martins, N.F., Strenkert, D., Clarke, C.A., Suchoszek, M., Thiele, W.,**
760 **Schöttler, M.A., and Merchant, S.S.** (2015). The thylakoid membrane protein
761 CGL160 supports CF1CF0 ATP synthase accumulation in Arabidopsis thaliana. PloS
762 one **10,** e0121658-e0121658.
763 **Gay, N.J.** (1984). Construction and characterization of an Escherichia coli strain with a uncI
764 mutation. Journal of bacteriology **158,** 820-825.
765 **Grahl, S., Reiter, B., Gügel, Irene L., Vamvaka, E., Gandini, C., Jahns, P., Soll, J.,**
766 **Leister, D., and Rühle, T.** (2016). The Arabidopsis Protein CGLD11 Is Required for
767 Chloroplast ATP Synthase Accumulation. Molecular Plant **9,** 885-899.
768 **Groth, G., and Pohl, E.** (2001). The structure of the chloroplast F1-ATPase at 3.2 A
769 resolution. The Journal of biological chemistry **276,** 1345-1352.
770 **Hahn, A., Vonck, J., Mills, D.J., Meier, T., and Kühlbrandt, W.** (2018). Structure,
771 mechanism, and regulation of the chloroplast ATP synthase. Science (New York,
772 N.Y.) **360,** eaat4318-eaat4318.
773 **He, J., Ford, H.C., Carroll, J., Douglas, C., Gonzales, E., Ding, S., Fearnley, I.M., and**
774 **Walker, J.E.** (2018). Assembly of the membrane domain of ATP synthase in human
775 mitochondria. Proceedings of the National Academy of Sciences, 201722086-
776 201722086.
777 **Hilbers, F., Eggers, R., Pradela, K., Friedrich, K., Herkenhoff-Hesselmann, B., Becker,**
778 **E., and Deckers-Hebestreit, G.** (2013). Subunit δ is the key player for assembly of

779 the H(+)-translocating unit of Escherichia coli F(O)F1 ATP synthase. The Journal of
780 biological chemistry **288,** 25880-25894.
781 **Ishihama, Y., Oda, Y., Tabata, T., Sato, T., Nagasu, T., Rappsilber, J., and Mann, M.**
782 (2005). Exponentially modified protein abundance index (emPAI) for estimation of
783 absolute protein amount in proteomics by the number of sequenced peptides per
784 protein. Mol Cell Proteomics **4,** 1265-1272.
785 **Junge, W., and Nelson, N.** (2015). ATP synthase. Annual Review of Biochemistry **84,** 631-
786 657.
787 **Kanazawa, A., and Kramer, D.M.** (2002). In vivo modulation of nonphotochemical exciton
788 quenching (NPQ) by regulation of the chloroplast ATP synthase. Proceedings of the
789 National Academy of Sciences of the United States of America **99,** 12789-12794.
790 **Kanazawa, A., Ostendorf, E., Kohzuma, K., Hoh, D., Strand, D.D., Sato-Cruz, M.,**
791 **Savage, L., Cruz, J.A., Fisher, N., Froehlich, J.E., and Kramer, D.M.** (2017).
792 Chloroplast ATP Synthase Modulation of the Thylakoid Proton Motive Force:
793 Implications for Photosystem I and Photosystem II Photoprotection. Frontiers in Plant
794 Science **8,** 1-12.
795 **Karimi, M., Inze, D., and Depicker, A.** (2002). GATEWAY vectors for Agrobacterium-
796 mediated plant transformation. Trends Plant Sci **7,** 193-195.
797 **Karpowicz, S.J., Prochnik, S.E., Grossman, a.R., and Merchant, S.S.** (2011). The
798 GreenCut2 Resource, a Phylogenomically Derived Inventory of Proteins Specific to
799 the Plant Lineage. Journal of Biological Chemistry **286,** 21427-21439.
800 **Kohzuma, K., Froehlich, J.E., Davis, G.A., Temple, J.A., Minhas, D., Dhingra, A., Cruz,**
801 **J.A., and Kramer, D.M.** (2017). The role of light–dark regulation of the chloroplast
802 ATP synthase. Frontiers in Plant Science **8,** 1-14.
803 **Liu, J., Hicks, D.B., and Krulwich, T.a.** (2013). Roles of AtpI and two YidC-type proteins
804 from alkaliphilic Bacillus pseudofirmus OF4 in ATP synthase assembly and
805 nonfermentative growth. Journal of bacteriology **195,** 220-230.
806 **Mao, J., Chi, W., Ouyang, M., He, B., Chen, F., and Zhang, L.** (2015). PAB is an assembly
807 chaperone that functions downstream of chaperonin 60 in the assembly of chloroplast
808 ATP synthase coupling factor 1. Proceedings of the National Academy of Sciences
809 **112,** 4152-4157.
810 **Merchant, S.S., Prochnik, S.E., Vallon, O., Harris, E.H., Karpowicz, S.J., Witman, G.B.,**
811 **Terry, A., Salamov, A., Fritz-Laylin, L.K., Maréchal-Drouard, L., Marshall, W.F.,**
812 **Qu, L.-H., Nelson, D.R., Sanderfoot, A.a., Spalding, M.H., Kapitonov, V.V., Ren,**
813 **Q., Ferris, P., Lindquist, E., Shapiro, H., Lucas, S.M., Grimwood, J., Schmutz, J.,**
814 **Cardol, P., Cerutti, H., Chanfreau, G., Chen, C.-L., Cognat, V., Croft, M.T., Dent,**
815 **R., Dutcher, S., Fernández, E., Fukuzawa, H., González-Ballester, D., González-**

816 **Halphen, D., Hallmann, A., Hanikenne, M., Hippler, M., Inwood, W., Jabbari, K.,**
817 **Kalanon, M., Kuras, R., Lefebvre, P.a., Lemaire, S.D., Lobanov, A.V., Lohr, M.,**
818 **Manuell, A., Meier, I., Mets, L., Mittag, M., Mittelmeier, T., Moroney, J.V.,**
819 **Moseley, J., Napoli, C., Nedelcu, A.M., Niyogi, K., Novoselov, S.V., Paulsen, I.T.,**
820 **Pazour, G., Purton, S., Ral, J.-P., Riaño-Pachón, D.M., Riekhof, W., Rymarquis,**
821 **L., Schroda, M., Stern, D., Umen, J., Willows, R., Wilson, N., Zimmer, S.L.,**
822 **Allmer, J., Balk, J., Bisova, K., Chen, C.-J., Elias, M., Gendler, K., Hauser, C.,**
823 **Lamb, M.R., Ledford, H., Long, J.C., Minagawa, J., Page, M.D., Pan, J.,**
824 **Pootakham, W., Roje, S., Rose, A., Stahlberg, E., Terauchi, A.M., Yang, P., Ball,**
825 **S., Bowler, C., Dieckmann, C.L., Gladyshev, V.N., Green, P., Jorgensen, R.,**
826 **Mayfield, S., Mueller-Roeber, B., Rajamani, S., Sayre, R.T., Brokstein, P.,**
827 **Dubchak, I., Goodstein, D., Hornick, L., Huang, Y.W., Jhaveri, J., Luo, Y.,**
828 **Martínez, D., Ngau, W.C.A., Otillar, B., Poliakov, A., Porter, A., Szajkowski, L.,**
829 **Werner, G., Zhou, K., Grigoriev, I.V., Rokhsar, D.S., and Grossman, A.R.** (2007).
830 The Chlamydomonas genome reveals the evolution of key animal and plant
831 functions. Science (New York, N.Y.) **318,** 245-250.
832 **Murphy, B.J., Klusch, N., Langer, J., Mills, D.J., Yildiz, O., and Kuhlbrandt, W.** (2019).
833 Rotary substates of mitochondrial ATP synthase reveal the basis of flexible F1-Fo
834 coupling. Science **364**.
835 **Naumenko, N., Morgenstern, M., Rucktaschel, R., Warscheid, B., and Rehling, P.**
836 (2017). INA complex liaises the F1Fo-ATP synthase membrane motor modules. Nat
837 Commun **8,** 1237.
838 **Obayashi, T., Hayashi, S., Saeki, M., Ohta, H., and Kinoshita, K.** (2009). ATTED-II
839 provides coexpressed gene networks for Arabidopsis. Nucleic acids research **37,**
840 D987-991.
841 **Omasits, U., Ahrens, C.H., Müller, S., and Wollscheid, B.** (2014). Protter: Interactive
842 protein feature visualization and integration with experimental proteomic data.
843 Bioinformatics **30,** 884-886.
844 **Ort, D.R., and Oxborough, K.** (1992). In Situ Regulation of Chloroplast Coupling Factor
845 Activity. Annual Review of Plant Physiology and Plant Molecular Biology **43,** 269-291.
846 **Ozaki, Y., Suzuki, T., Kuruma, Y., Ueda, T., and Yoshida, M.** (2008). UncI protein can
847 mediate ring-assembly of c-subunits of FoF1-ATP synthase in vitro. Biochemical and
848 biophysical research communications **367,** 663-666.
849 **Peng, L., Shimizu, H., and Shikanai, T.** (2008). The chloroplast NAD(P)H dehydrogenase
850 complex interacts with photosystem I in Arabidopsis. The Journal of biological
851 chemistry **283,** 34873-34879.

852 **Pettersen, E.F., Goddard, T.D., Huang, C.C., Meng, E.C., Couch, G.S., Croll, T.I., Morris,**
853 **J.H., and Ferrin, T.E.** (2021). UCSF ChimeraX: Structure visualization for
854 researchers, educators, and developers. Protein Science **30,** 70-82.
855 **Pfalz, J., Bayraktar, O.A., Prikryl, J., and Barkan, A.** (2009). Site-specific binding of a PPR
856 protein defines and stabilizes 5' and 3' mRNA termini in chloroplasts. The EMBO
857 journal **28,** 2042-2052.
858 **Porra, R.J., Thompson, W.A., and Kriedemann, P.E.** (1989). Determination of accurate
859 extinction coefficients and simultaneous equations for assaying chlorophylls a and b
860 extracted with four different solvents: verification of the concentration of chlorophyll
861 standards by atomic absorption spectroscopy. Biochim Biophys Acta **975,** 384-394.
862 **Rappsilber, J., Ishihama, Y., and Mann, M.** (2003). Stop and go extraction tips for matrix-
863 assisted laser desorption/ionization, nanoelectrospray, and LC/MS sample
864 pretreatment in proteomics. Anal Chem **75,** 663-670.
865 **Reiland, S., Messerli, G., Baerenfaller, K., Gerrits, B., Endler, A., Grossmann, J.,**
866 **Gruissem, W., and Baginsky, S.** (2009). Large-scale Arabidopsis phosphoproteome
867 profiling reveals novel chloroplast kinase substrates and phosphorylation networks.
868 Plant physiology **150,** 889-903.
869 **Reiland, S., Finazzi, G., Endler, A., Willig, A., Baerenfaller, K., Grossmann, J., Gerrits,**
870 **B., Rutishauser, D., Gruissem, W., Rochaix, J.-D., and Baginsky, S.** (2011).
871 Comparative phosphoproteome profiling reveals a function of the STN8 kinase in
872 fine-tuning of cyclic electron flow (CEF). Proceedings of the National Academy of
873 Sciences of the United States of America **108,** 12955-12960.
874 **Reiter, B., Vamvaka, E., Marino, G., Kleine, T., Jahns, P., Bolle, C., Leister, D., and**
875 **Rühle, T.** (2020). The Arabidopsis Protein CGL20 Is Required for Plastid 50S
876 Ribosome Biogenesis. Plant physiology **182,** 1222-1238.
877 **Robinson, G.C., Bason, J.V., Montgomery, M.G., Fearnley, I.M., Mueller, D.M., Leslie,**
878 **A.G., and Walker, J.E.** (2013). The structure of F(1)-ATPase from Saccharomyces
879 cerevisiae inhibited by its regulatory protein IF(1). Open Biol **3,** 120164.
880 **Roitinger, E., Hofer, M., Kocher, T., Pichler, P., Novatchkova, M., Yang, J.,**
881 **Schlogelhofer, P., and Mechtler, K.** (2015). Quantitative phosphoproteomics of the
882 ataxia telangiectasia-mutated (ATM) and ataxia telangiectasia-mutated and rad3-
883 related (ATR) dependent DNA damage response in Arabidopsis thaliana. Mol Cell
884 Proteomics **14,** 556-571.
885 **Rühle, T., and Leister, D.** (2015). Assembly of F1F0-ATP synthases. Biochimica et
886 Biophysica Acta (BBA) - Bioenergetics **1847,** 849-860.

887 **Rühle, T., Dann, M., Reiter, B., Schünemann, D., Naranjo, B., Penzler, J.-f., Kleine, T.,**
888 **and Leister, D.** (2021). PGRL2 triggers degradation of PGR5 in the absence of
889 PGRL1. Nature communications **12,** 3941-3941.
890 **Rühle, T., Razeghi, J.A., Vamvaka, E., Viola, S., Gandini, C., Kleine, T., Schünemann,**
891 **D., Barbato, R., Jahns, P., and Leister, D.** (2014). The Arabidopsis protein
892 CONSERVED ONLY IN THE GREEN LINEAGE160 promotes the assembly of the
893 membranous part of the chloroplast ATP synthase. Plant physiology **1. Wittenb,** 207-
894 226.
895 **Schägger, H.** (2006). Tricine-SDS-PAGE. Nature protocols **1,** 16-22.
896 **Schöttler, M.A., Tóth, S.Z., Boulouis, A., and Kahlau, S.** (2014). Photosynthetic complex
897 stoichiometry dynamics in higher plants: biogenesis, function, and turnover of ATP
898 synthase and the cytochrome b 6 f complex. Journal of experimental botany.
899 **Schreiber, U., and Klughammer, C.** (2008). New accessory for the Dual-PAM-100 : The
900 P515 / 535 module and examples of its application. PAM Application Notes **10,** 1-10.
901 **Sobti, M., Smits, C., Wong, A.S., Ishmukhametov, R., Stock, D., Sandin, S., and**
902 **Stewart, A.G.** (2016). Cryo-EM structures of the autoinhibited E. coli ATP synthase in
903 three rotational states. Elife **5,** 1-18.
904 **Song, J., Pfanner, N., and Becker, T.** (2018). Assembling the mitochondrial ATP synthase.
905 Proceedings of the National Academy of Sciences of the United States of America
906 **115,** 2850-2852.
907 **Spitzer, M., Wildenhain, J., Rappsilber, J., and Tyers, M.** (2014). BoxPlotR: a web tool for
908 generation of box plots. Nat Methods **11,** 121-122.
909 **Suzuki, T., Ozaki, Y., Sone, N., Feniouk, B.a., and Yoshida, M.** (2007). The product of uncI
910 gene in F1Fo-ATP synthase operon plays a chaperone-like role to assist c-ring
911 assembly. Proceedings of the National Academy of Sciences of the United States of
912 America **104,** 20776-20781.
913 **Takabayashi, A., Takabayashi, S., Takahashi, K., Watanabe, M., Uchida, H., Murakami,**
914 **A., Fujita, T., Ikeuchi, M., and Tanaka, A.** (2017). PCoM-DB update: A protein co-
915 migration database for photosynthetic organisms. Plant and Cell Physiology **58,** e10-
916 e10.
917 **Tanigawara, M., Tabata, K.V., Ito, Y., Ito, J., Watanabe, R., Ueno, H., Ikeguchi, M., and**
918 **Noji, H.** (2012). Role of the DELSEED loop in torque transmission of F1-ATPase.
919 Biophys J **103,** 970-978.
920 **Tomizioli, M., Lazar, C., Brugiere, S., Burger, T., Salvi, D., Gatto, L., Moyet, L., Breckels,**
921 **L.M., Hesse, A.M., Lilley, K.S., Seigneurin-Berny, D., Finazzi, G., Rolland, N., and**
922 **Ferro, M.** (2014). Deciphering Thylakoid Sub-compartments using a Mass
923 Spectrometry-based Approach. Molecular & Cellular Proteomics **13,** 2147-2167.

924 **Trosch, R., Topel, M., Flores-Perez, U., and Jarvis, P.** (2015). Genetic and Physical
925 Interaction Studies Reveal Functional Similarities between ALBINO3 and ALBINO4 in
926 Arabidopsis. Plant physiology **169,** 1292-1306.
927 **Vollmar, M., Schlieper, D., Winn, M., Büchner, C., and Groth, G.** (2009). Structure of the
928 c14 rotor ring of the proton translocating chloroplast ATP synthase. The Journal of
929 biological chemistry **284,** 18228-18235.
930 **von Ballmoos, C., Wiedenmann, A., and Dimroth, P.** (2009). Essentials for ATP synthesis
931 by F1F0 ATP synthases. Annual review of biochemistry **78,** 649-672.
932 **Yap, A., Kindgren, P., Colas Des Francs-Small, C., Kazama, T., Tanz, S.K., Toriyama,**
933 **K., and Small, I.** (2015). AEF1/MPR25 is implicated in RNA editing of plastid atpF
934 and mitochondrial nad5, and also promotes atpF splicing in Arabidopsis and rice.
935 Plant Journal **81,** 661-669.
936 **Zhang, L., Rochaix, J.D., and Peng, L.** (2020). Regulation of the biogenesis of chloroplast
937 ATP synthase. Advances in Botanical Research **96,** 205-228.
938 **Zhang, L., Duan, Z., Zhang, J., and Peng, L.** (2016). BIOGENESIS FACTOR REQUIRED
939 FOR ATP SYNTHASE 3 Facilitates Assembly of the Chloroplast ATP Synthase
940 Complex in Arabidopsis. Plant Physiology **171,** pp.00248.02016-pp.00248.02016.
941 **Zhang, L., Zhou, W., Che, L., Rochaix, J.D., Lu, C., Li, W., and Peng, L.** (2019). PPR
942 Protein BFA2 Is Essential for the Accumulation of the atpH/F Transcript in
943 Chloroplasts. Front Plant Sci **10,** 446.
944 **Zhang, L., Pu, H., Duan, Z., Li, Y., Liu, B., Zhang, Q., Li, W., Rochaix, J.-D., Liu, L., and**
945 **Peng, L.** (2018). Nucleus-Encoded Protein BFA1 Promotes Efficient Assembly of the
946 Chloroplast ATP Synthase Coupling Factor 1. The Plant Cell **30,** 1770-1788.
947 **Zoschke, R., Kroeger, T., Belcher, S., Schöttler, M.A., Barkan, A., and Schmitz-**
948 **Linneweber, C.** (2012). The pentatricopeptide repeat-SMR protein ATP4 promotes
949 translation of the chloroplast atpB/E mRNA. The Plant journal : for cell and molecular
950 biology **72,** 547-558.

951

952 ## Supplemental tables

953 **Supplemental Table S1. AtCGL160 co-immunoprecipitation experiments.** Differential
954 enriched proteins in *P_{35S}:AtCGL160* versus *P_{35S}:AtCGL160C* samples sorted by $\log_2$ fold
955 change ($-\log_{10}$ *P*-value > 1.5). Nucleus-encoded genes are written in capital letters.

Protein IDs (Uniprot)	Gene names	$\log_2$ FC	$-\log_{10}$ p-value
O82279	*AtCGL160*	6.495	4.644
P09468	*atpE*	6.38	2.301
Q42139	*ATPG*	5.231	4.747
P56760	*atpH*	4.886	3.176
Q9SSS9	*ATPD*	4.672	4.523
P19366	*atpB*	4.437	4.459
P56759	*atpF*	4.399	5.913
P56757	*atpA*	4.235	6.41
Q01908	*ATPC1*	4.156	4.772
Q2HIU0	*At3g15110*	3.333	3.508
P56758	*atpI*	2.799	4.104
O49445	*LECRK72*	2.346	3.115
Q67XC4	*TBL40*	2.268	2.402
Q8LCQ4	*LHCA6*	2.082	3.71
A0A1P8B288, Q39099	*XTH4*	1.983	4.126
Q41963	*TIP1-2*	1.907	2.821
O22957	*At2g34040*	1.632	2.829
Q9SRL2, Q9M9X0, F4J8G2, Q9SRL7, Q9S9U3	*RLP32, RLP33, RLP34, RLP35, RLP53*	1.564	3.162
P38418, A0A1I9LPH1	*LOX2*	1.544	2.047
Q8LBV4	*At1g78140*	1.515	2.171
F4IUJ0, F4IUI9	*At2g26340*	1.451	3.021
Q9SF53, A0A1I9LSB4, Q9M3D2	*RPL35A, RPL35C*	1.254	2.619
A0A1P8B6D0, Q9SUI4	*PSAL*	1.193	2.938
Q9FFW9, F4KBJ3	*At5g38520*	1.136	3.084
Q96242	*CYP74A*	1.078	2.371
Q9SYW8, F4K8I1	*Lhca2*	0.941	2.356
Q9SR92	*STR10*	0.839	2.913
P56777	*psbB*	0.807	2.072
Q9LHA6	*At3g28220*	0.731	2.315
Q9S7N7	*PSAG*	0.575	2.157

956

957 **Supplemental Table S2. Primers used in this study.**

Primer name	Primer sequence 5' to 3'	Comment
oeAtCGL160_s	GGGGACAAGTTTGTACAAAAAAGCAGGCTCAATGGCGATTCTTAGTTACAT	Gateway primer
oeAtCGL160_as	GGGGACCACTTTGTACAAGAAAGCTGGGTTTAATCACTGGCCTGTGTGT	Gateway primer
oeAtCGL160C_s	GGGGACAAGTTTGTACAAAAAAGCAGGCTCAatgGAACAATATTTTAAGCTGAAAA	Gateway primer
TP-GC9C_fus_s	GGTCCACCGGAGTTGCTCCCGAACAATATTTTAAGCTGAA	Fusion PCR
TP-Gc9C_fus_as	TTCAGCTTAAAATATTGTTCGGGAGCAACTCCGGTGGACC	Fusion PCR
CGL160-MBP_s	AAAATCATTCTACCCAATAA	MBP cloning primer
CGL160N-MBP_as	GGTCCTGAATTCTTACCTGTCTTTAGCAGCTTGTA	MBP cloning primer
GST-CGL160N-s	GGGGACAAGTTTGTACAAAAAAGCAGGCTCAAAAATCATTCTACCCAATAAGAAACCTGA	Gateway primer
GST-CGL160N-as	GGGGACCACTTTGTACAAGAAAGCTGGGTCTTACCTGTCTTTAGCAGCTTGTAC	Gateway primer
cgl160cTP_probe_s	ATGGCGATTCTTAGTTACATCTCAGC	Northern-probe
cgl160cTP_probe_as	GGGAGCAACTCCGGTG	Northern-probe
pGBKT7-CGL160N_s	GGTGGTCATATGAAAATCATTCTACCCAATAAGA	Y2H cloning primer
pGBKT7-CGL160N_as	GGTCCTGAATTCTTACCTGTCTTTAGCAGCTTGTA	Y2H cloning primer
pGADT7-alpha_s	GGTGGTCATATGGTAACCATTAGAGCCGACGA	Y2H cloning primer
pGADT7-alpha_as	GGTCCTGAATTCTTATACTTTCTCCTGAAGTA	Y2H cloning primer
pGADT7-beta_s	GGTGGTCATATGAGAACAAATCCTACTACTTC	Y2H cloning primer
pGADT7-beta_as	GGTCCTGAATTCTCATTTCTTCAATTTACTCT	Y2H cloning primer
pGADT7-gamma_s	GGTGGTCATATGGCTTCCTCTGTTTCACCACT	Y2H cloning primer
pGADT7-gamma_as	GGTCCTGAATTCTCAAACCTGTGCATTAGCTC	Y2H cloning primer
pGADT7-delta_s	GGTGGTCATATGGCCACCGCAGCATCAAGCTA	Y2H cloning primer
pGADT7-delta_as	GGTCCTGAATTCTCAAGTAGCTAATTGAATCT	Y2H cloning primer

pGADT7-epsilon_s	GGTGGTCATATGACCTTAAATCTTTGTGTACTGACTC	Y2H cloning primer
pGADT7-epsilon_as	GGTCCTGAATTCTCAAATCGTATTGAGAGCCT	Y2H cloning primer
pGADT7-AtCGL160_s	GGTGGTCATATGAAAATCATTCTACCCAATAAGA	Y2H cloning primer
pGADT7-AtCGL160_as	GGTCCTGAATTCTTACCTGTCTTTAGCAGCTTGTA	Y2H cloning primer
pGADT7-AtCGLD11_s	GGTGGTCATATGTCTTCGAGTCTATGGAAGCT	Y2H cloning primer
pGADT7-AtCGLD11_as	GGTCCTGAATTCTTAACCCTGGAGTAATTTCA	Y2H cloning primer
pGADT7-atpFsoluble_s	GGTGGTCATATGGATTTATTAGATAACCGAAAG	Y2H cloning primer
pGADT7-atpFsoluble_as	GGTCCTGAATTCTTAATCAGTTATTTCTTTCATCG	Y2H cloning primer
pGADT7-atpGsoluble_s	GGTGGTCATATGCCGCTTGGTAACTTCATGG	Y2H cloning primer
pGADT7-atpGsoluble_as	GGTCCTGAATTCTTAAGAAGGAAGAACCTTCTTGAC	Y2H cloning primer
pGADT7_AtpBI-AD_s	CGCGAATTCATGAGAACAAATCCTAC	Y2H cloning primer
pGADT7_AtpBI-AD_as	ACTCTCGAGTCAATTTCCCATATCAACCAC	Y2H cloning primer
pGADT7_AtpBII-AD_s	ATGGAATTCCCTCTAAGTGTTCCAG	Y2H cloning primer
pGADT7_AtpBII-AD_as	AACCTCGAGTCAAGGTTGTAGCATAGTTG	Y2H cloning primer
pGADT7_AtpBIII-AD_s	CTAGAATTCCGAATCGTTGGCGAG	Y2H cloning primer
pGADT7_AtpBIII-AD_as	GCGCTCGAGTCATTTCTTCAATTTACTC	Y2H cloning primer
pGBKT7_CGL160N_del29_74_s	GACTTAATCTGGAACAGAGATTTTATGG	Y2H cloning primer
pGBKT7_CGL160N_del29_74_as	CATATGCAGGTCCTCCTCT	Y2H cloning primer
pGBKT7_CGL160N_del75_105_s	GTCTTCTGGGTTTCTGAG	Y2H cloning primer
pGBKT7_CGL160N_del75_105_as	GTGGAAGTAATGGGATCTTC	Y2H cloning primer
pGBKT7_CGL160N_del106_134_s	CGTTGTGAAAAATCGTCTTGACAC	Y2H cloning primer
pGBKT7_CGL160N_del106_134_as	GACTTTTCCTTTGAAGGAGATGG	Y2H cloning primer
pGBKT7_CGL160N_del135_160_s	GAAGCTGGCACCTACACG	Y2H cloning primer
pGBKT7_CGL160N_del135_160_as	CATTTAGAAGACGATGCAAGCTCTTTACTTAAATC	Y2H cloning primer
pGBKT7_CGL160N_del161_206_s	GAATTCCCGGGGATCCG	Y2H cloning primer
pGBKT7_CGL160N_del161_206_as	CTATTTAGGAGACACAATAGCCTTACTCATTTG	Y2H cloning primer

958

Supplemental Figures

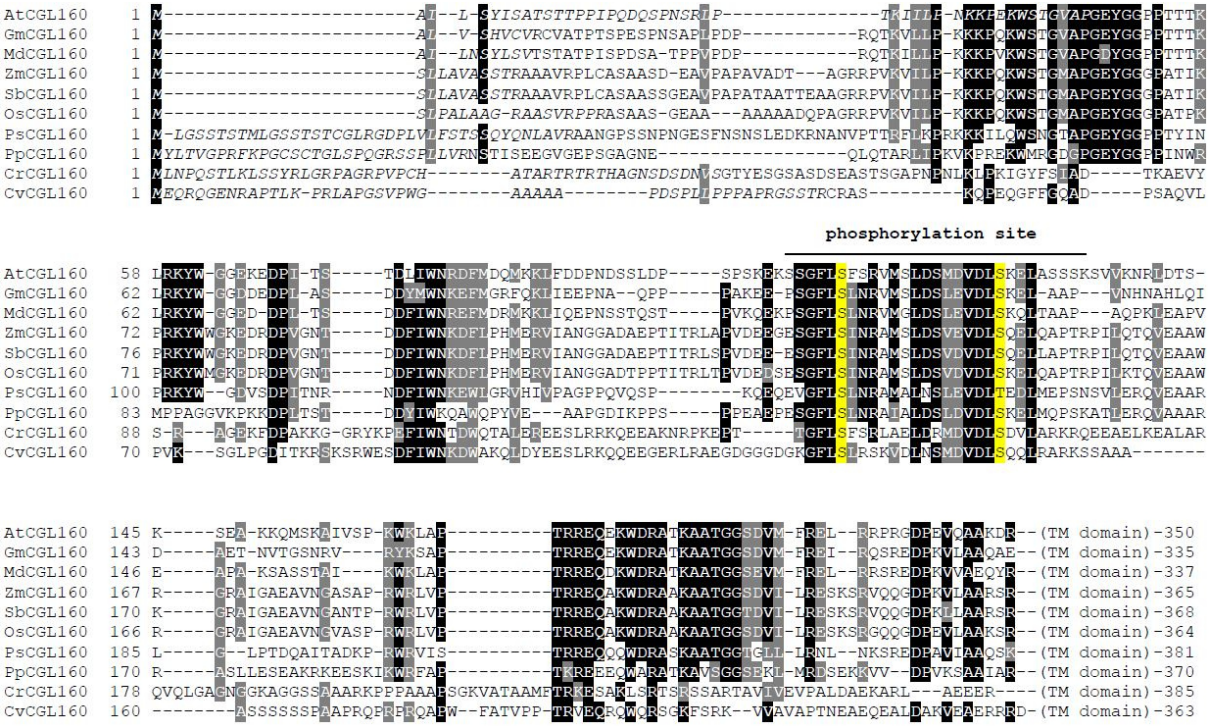

Supplemental Figure S1. **Multiple alignment of the N-terminal portions of CGL160 sequences identified in species belonging to the green lineage.** Chloroplast transit peptides predicted by ChloroP are depicted in italics. Similar and identical amino acids conserved in 70% of the sequences are highlighted in grey and black, respectively. The region that includes several identified phosphopeptides in AtCGL160 is indicated and two conserved S/T residues are shown in yellow. Note that CGL160 transmembrane (TM) domains were omitted from the alignment. Sequence identifiers for CGL160 homologs are as follows: *Arabidopsis thaliana* (AtCGL160, NP_565711), *Glycine max* (GmCGL160, XP_006582279.1), *Malus domestica* (MdCGL160, XP_008353735.1), *Zea mays* (ZmCGL160, NP_001170362.2), *Sorghum bicolor* (SmCGL160, XP_021312638.1), *Oryza sativa* Japonica group (OsCGL160, XP_015619276.1), *Picea sitchensis* (PsCGL160, ABR16992.1), *Physcomitrella patens* (PpCGL160, XP_024381807.1), *Chlamydomonas reinhardtii* (CrCGL160, XP_001690237.1) and *Chlorella variabilis* (CvCGL160, XP_005844436.1).

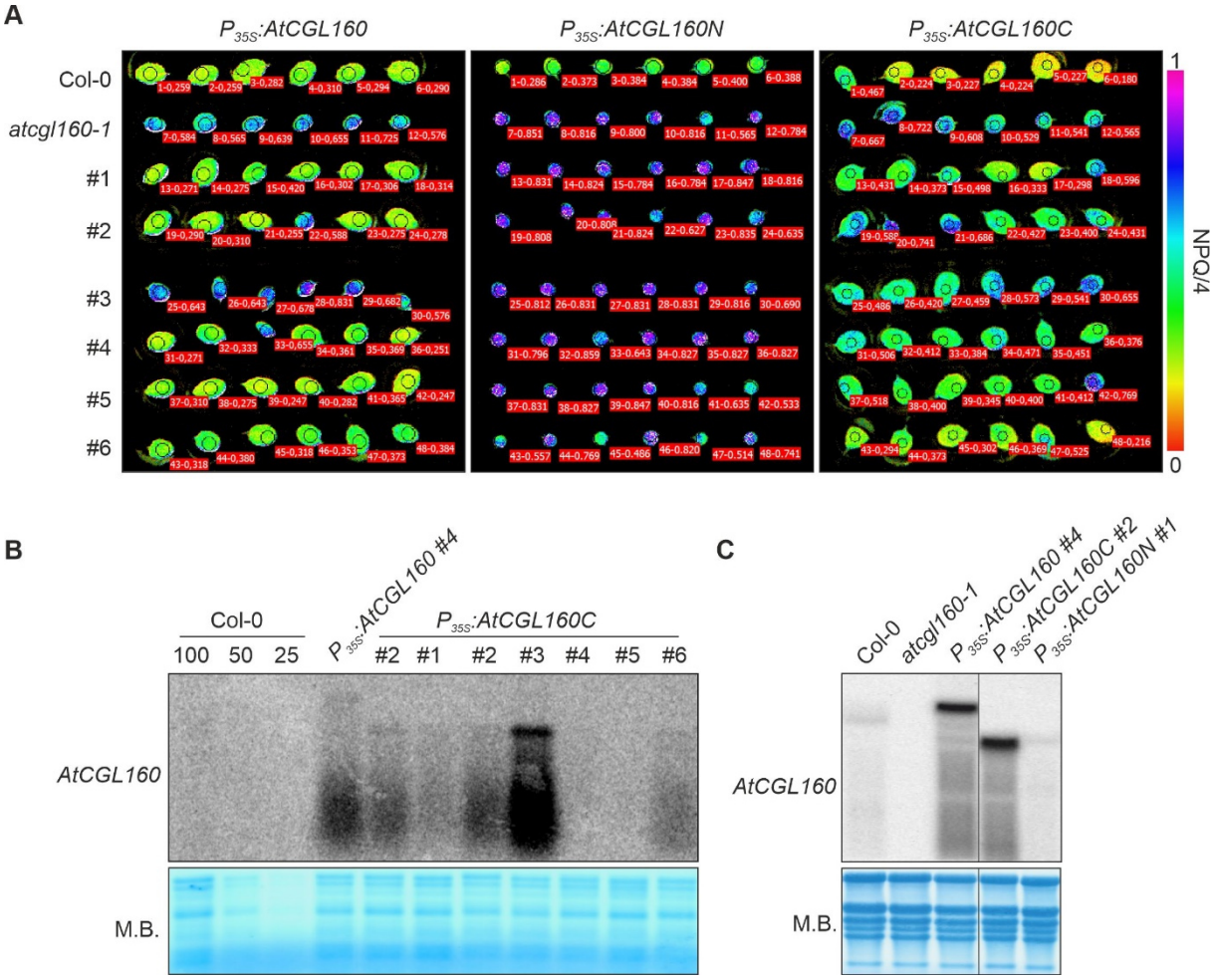

Supplemental Figure S2. Screening of *P_{35S}:AtCGL160, P_{35S}:AtCGL160N* and *P_{35S}:AtCGL160C* plants. A, After transformation of *atcgl160-1*, T2 offspring of independent T1 plants (#1-#6) were examined using an Imaging-PAM (Walz, Effeltrich, Germany) system. Non-photochemical quenching (NPQ/4) was measured in light induction experiments on detached leaves after 8 min of irradiation at 100 µmol photons m^{-2} s^{-1}, and is indicated on a false-color scale from 0 to 1. Col-0 and *atcgl160-1* leaves served as controls. *P_{35S}:AtCGL160* lines #1, #2, #4, #5 and #6 rescued the *atcgl160-1* phenotype. Transformation of *atcgl160-1* plants with the *P_{35S}:AtCGL160N* and *P_{35S}:AtCGL160C* constructs resulted in no complementation and partial complementation, respectively. **B**, *AtCGL160* transcript levels in *P_{35S}:AtCGL160C* plants determined by Northern analysis. Note that RNA samples (8 µg) of line #2 were loaded twice for direct comparison of transcript levels with line #1 (*P_{35S}:AtCGL160*). **C**, Northern analyses of selected, homozygous lines (T3 generation). Total RNA (20 µg) from 4-week-old Col-0, *atcgl160-1*, *P_{35S}:AtCGL160, P_{35S}:AtCGL160N* and *P_{35S}:AtCGL160C* plants was size-fractionated on a denaturing formaldehyde gel and blotted onto a nylon membrane. Hybridization was carried out with a radioactive probe specific for the *AtCGL160* chloroplast transit-peptide coding region. Line #4 (*P_{35S}:AtCGL160)* and line #2 (*P_{35S}:AtCGL160C)* were selected for further experiments due to their similar transcript levels. Methylene blue (M.B.) staining of the nylon membrane served as an RNA loading control in **B** and **C**.

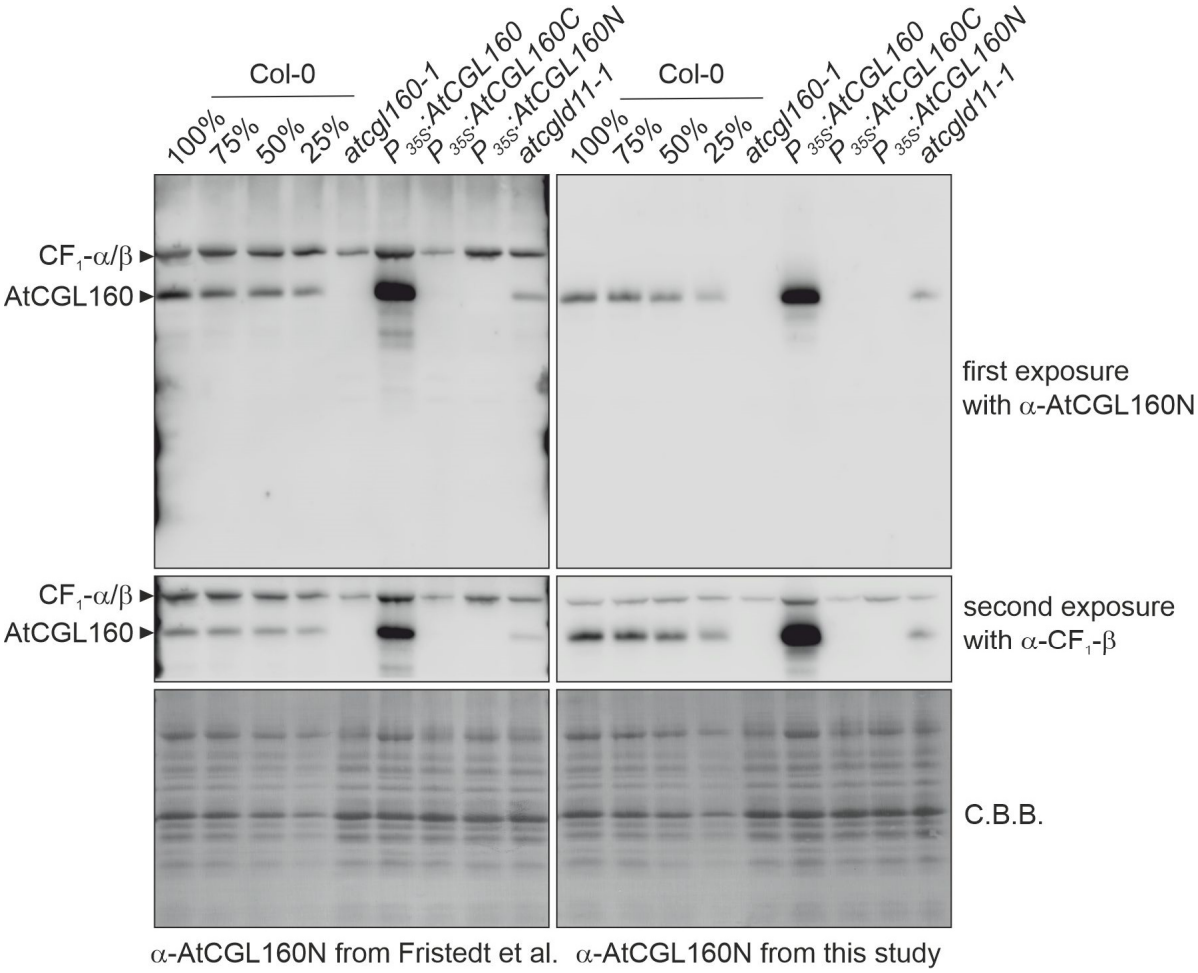

Supplemental Figure S3. Immunodetection of AtCGL160 in Col-0, *atcgl160-1*, *P_{35S}:AtCGL160, P_{35S}:AtCGL160N, P_{35S}:AtCGL160C* and *atcgld11-1* plants. Thylakoid proteins were separated by denaturing SDS-PAGE and blotted onto PVDF membranes. Membranes were first probed with antibodies against AtCGL160N. After signal detection, membranes were re-probed with an antibody against CF_1-β. Coomassie brilliant blue staining (C.B.B.) of PVDF membranes is shown as a loading control. On the left, immunodetection analyses are shown for an AtCGL160 antibody (AS12 1853) which is commercially available from Agrisera and was employed in Fristedt et al. (2015). A side-by-side comparison with the newly generated antibody against the N-terminal part of AtCGL160 is provided in the right panel. Note that antibody AS12 1853 from Agrisera binds nonspecifically to CF_1-α or CF_1-β and was therefore not considered for use in co-immunoprecipitation, cross-linking or 2D native/SDS-PAGE experiments.

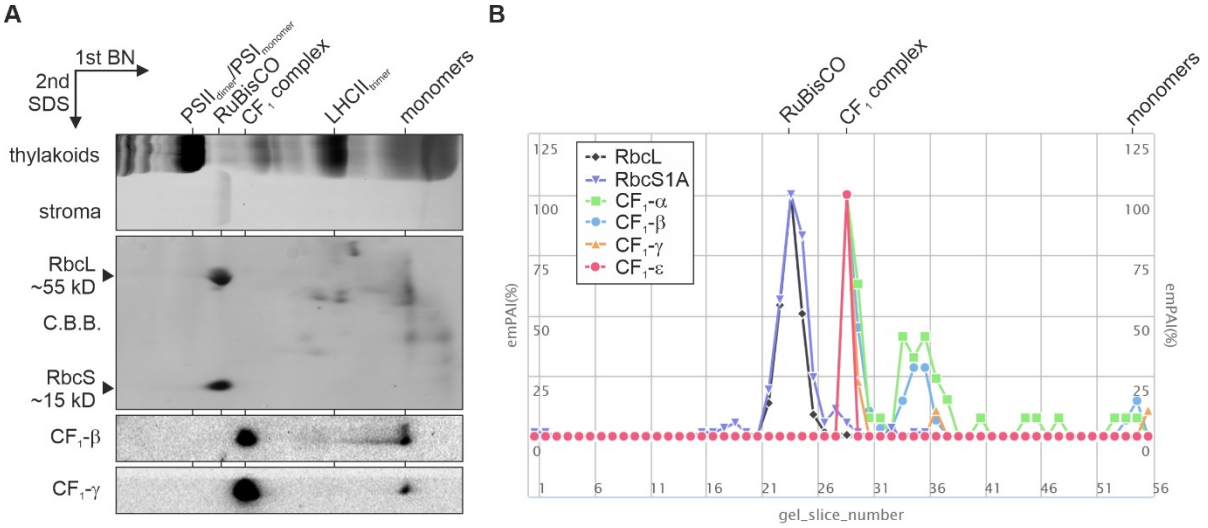

Supplemental Figure S4. Characterization of the stromal CF_1 complex in *atcgl160-1* plants. **A**, A stromal protein extract of *atcgl160-1* plants was subjected to 2D gel electrophoresis (Blue Native- and SDS-PAGE) and immunodetection of CF_1-β and CF_1-γ. Coomassie brilliant blue (G-250) staining of the PVDF membrane after transfer visualized abundant stromal complexes such as RuBisCO, which is composed of RbcL and RbcS. Prominent thylakoid complexes of *P_{35S}:AtCGL160C* plants served as molecular mass standards. **B**, Composition of the stromal CF_1 sub-complex in Arabidopsis according to the Protein Co-migration Database for photosynthetic organisms (PCom-DB, http://pcomdb.lowtem.hokudai.ac.jp/proteins/top). Co-migration of RbcL (black diamonds) and RbcS (purple triangles) is provided for better comparison between PCom-DB results and the 2D gel analyses presented in panel **A**. Subunit content is quantified according to the exponentially modified protein abundance index (emPAI) method and is normalized for each individual subunit to the maximal emPAI identified in a gel slice (Ishihama et al., 2005). The maximal RuBisCO and CF_1 content was detected in gel slices 24 and 29, respectively. Note that CF_1-δ was not identified in the stromal CF_1 subcomplex.

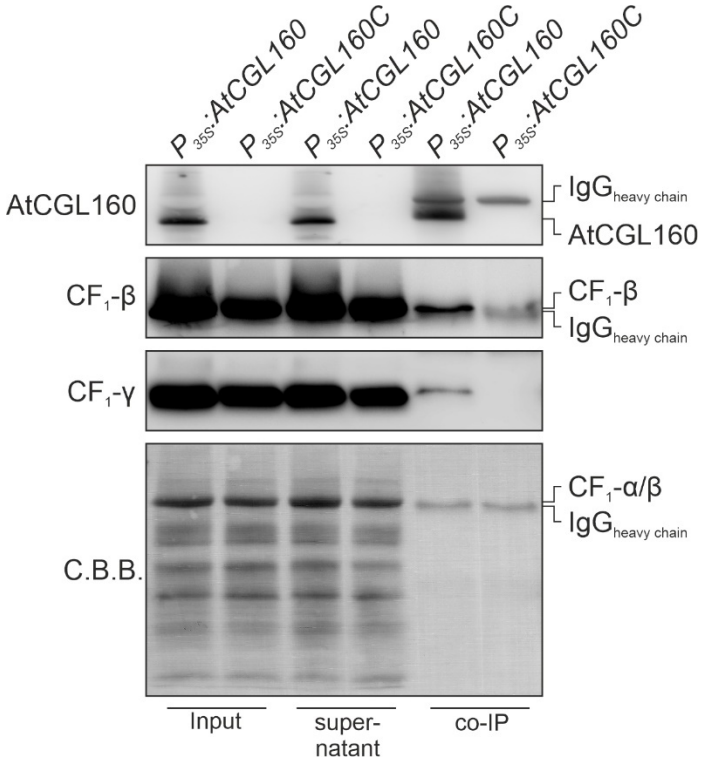

Supplemental Figure S5. Immunoblot analysis of AtCGL160 co-immunoprecipitation assays. A, Co-immunoprecipitation with NP40-solubilized thylakoids of oeAtCGL160 and oeAtCGL160C was repeated using reduced amounts of the AtCGL160 antibody. Protein A-coupled magnetic beads (Dynabeads, Thermo) coated with AtCGL160 antibody and co-immunoprecipated proteins (IP) were boiled in SDS loading buffer, separated by denaturing SDS-PAGE and blotted onto PVDF membranes. Samples of NP40-solubilized thylakoids before (Input) and after (Flow) incubation with AtCGL160 antibody were loaded as controls. Membranes were probed separately with antibodies against AtCGL160N and CF_1-β/CF_1-γ. The positions of the heavy chain of the AtCGL160 antibody are indicated (IgG). Coomassie brilliant blue staining (C.B.B.) is shown as loading control, and the positions of CF_1-α/β are indicated.

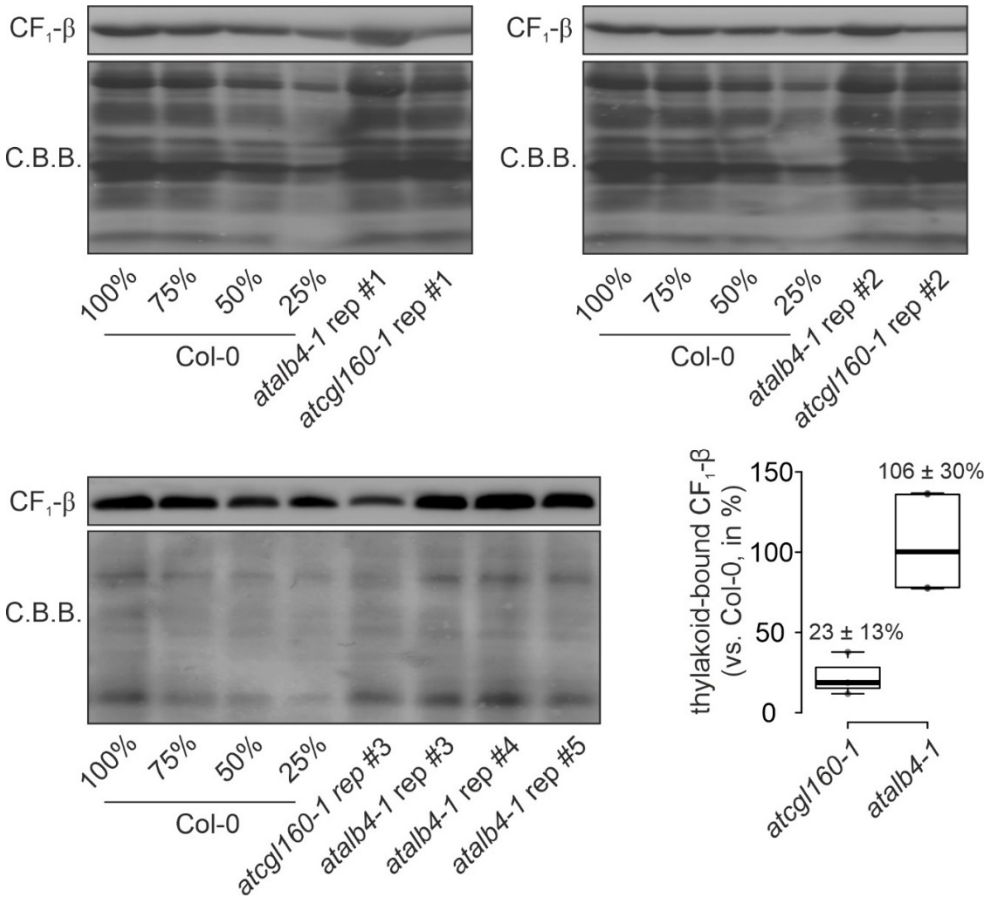

Supplemental Figure S6. Quantification of thylakoid-bound CF_1-β subunits in *atalb4-1* Arabidopsis mutant lines. Thylakoid proteins were isolated from Col-0, *atcgl160-1* and *atalb4-1* (SALK_136199C) plants grown under short-day conditions, fractionated on SDS-PAGE, transferred to PVDF membranes and probed with CF_1-β antibodies. Membranes were stained with Coomassie brilliant blue G-250 (C.B.B.) as loading control. Signals were quantified relative to signals detected in the wild-type sample using the Bio-1D software (version 15.03, Vilber Lourmat, Eberhardzell, Germany) and are provided as percentages. Horizontal lines represent the median, and boxes indicate the 25th and 75th percentiles. Whiskers extend the interquartile range by a factor of 1.5×. Means ± standard deviations are provided above the boxes. Quantification is based on three and five replicates (rep) for *atcgl160-1* and *atalb4-1* samples, respectively.

Additional references in Supplemental Figures

Ishihama, Y., Oda, Y., Tabata, T., Sato, T., Nagasu, T., Rappsilber, J., and Mann, M. (2005). Exponentially modified protein abundance index (emPAI) for estimation of absolute protein amount in proteomics by the number of sequenced peptides per protein. Mol Cell Proteomics **4,** 1265-1272.